TECHNICAL REPORT No. 29

OVERCOMING RHEOTROPIC EMBRITTLEMENT
BY TORSIONAL PRESTRAIN

An Investigation of
THE EFFECTS OF STRESS CONCENTRATION AND
TRIAXIALITY ON THE PLASTIC FLOW OF METALS

Technical Report No. 29
OVERCOMING RHEOTROPIC EMBRITTLEMENT
BY TORSIONAL PRESTRAIN

By

I. Rozalsky

Conducted By
METALS RESEARCH LABORATORY
DEPARTMENT OF METALLURGICAL ENGINEERING
CASE INSTITUTE OF TECHNOLOGY

Cleveland, Ohio

June, 1954

METALS RESEARCH LABORATORY

DEPARTMENT OF METALLURGICAL ENGINEERING

CASE INSTITUTE OF TECHNOLOGY

Technical Report No. 29

OVERCOMING RHEOTROPIC EMBRITTLEMENT
BY TORSIONAL PRESTRAIN

Written by

Y. Rozalsky

I. Rozalsky

Approved by

W. ⅂ᶜ. Baldwin, Jr.

Task Order Director

Distribution List for
Technical Report
No. 29

Copy No._____

Contract N6-onr-273/1   June 1954   Project NR-031-049

Copy No.

1-2	Chief of Naval Research Department of the Navy Washington 25, D.C. Attn: Code 423	9-14	Director, Naval Res. Lab. Washington 25, D.C. Att: Technical Information Officer
3	Commanding Officer Office of Naval Research Branch Office 50 Church Street New York 7, N.Y.	15	Dr. C. S. Smith Institute for the Study of Metal University of Chicago Chicago, Illinois
4	Commanding Officer Office of Naval Research Branch Office The John Crerar Library Bldg. 10th Floor 86 E. Randolph Street Chicago 11, Illinois	16-17	University of California Engineering Department Berkeley, California Att: Dr. J. E. Dorn Dr. E. R. Parker
		18	Professor F. A. Biberstein Department of Mech. Engr. Catholic University of America Washington, D.C.
5	Commanding Officer Office of Naval Research Branch Office 801 Donahue Street San Francisco 24, Calif.	19	Professor W. Prager School of Applied Mathematics Brown University Providence, Rhode Island
6	Commanding Officer Office of Naval Research Branch Office 1030 Green Street Pasadena, California	20	Dr. L. V. Griffis Applied Mechanics Division Armour Research Foundation Chicago, Illinois
7	Assistant Naval Attache for Research London, England U. S. Navy FPO #100 New York, N.Y.	21	Dr. W. C. MacGregor Dept. of Mech. Engr. Massachusetts Inst. of Tech. Cambridge, Massachusetts
8	Contract Administrator, SE Area, Office of Naval Res. Department of the Navy Washington 25, D.C. Att: Mr. R. F. Lynch	22	Director David Taylor Model Basin Washington 7, D. C.

23	Armour Research Foundation Metals Research Division 35 W. 33rd Street Chicago, Illinois Att: W. E. Mahin	42	U. S. Naval Engineering Experiment Station Annapolis, Maryland Attn: Metals Laboratory
24-25	Director, Naval Res. Laboratory Washington 25, D. C. Attn: Code 2500, Metallurgy Code 2020, Tech. Library	43	Director, Materials Laboratory Building 291 New York Naval Shipyard Brooklyn 1, New York Attn: Code 907
26-29	Bureau of Aeronautics Department of the Navy Washington 25, D. C. Attn: N. E. Promisel, AE-41(3) Technical Library, TD-41(1)	44	Bureau of Yards and Docks Department of the Navy Washington 25, D. C. Attn: Research & Standards Div.

ARMY

30	Commanding Officer Naval Air Material Center Naval Base Station Philadelphia, Penna. Attn: Aeronautical Materials Laboratory	45	Chief of Staff, U. S. Army The Pentagon Washington 25, D. C. Attn: Director of Research & Development
31-34	Bureau of Ordnance Department of the Navy Washington 25, D. C. Attn: Rex (3) Technical Library AD3(1)	46-48	Office of Chief of Ordnance Research & Development Service Department of the Army Washington 25, D. C. Attn: ORDTB
35	Superintendent, Naval Gun Factory Washington 20, D. C. Attn: Metallurgical Lab IN910	49	Commanding Officer Frankfod Arsenal Philadelphia 37, Pa.
36	Commanding Officer U. S. Naval Ordnance Test Station Inyokern, California	50	Commanding Officer Watertown Arsenal Watertown, Massachusetts Attn: Laboratory
37-40	Bureau of Ships Department of the Navy Washington 25, D. C. Attn: Code 343 (3) Code 337L, Tech. Lib. (1)	51	Office of Chief of Engineers Department of the Army Washington 25, D. C. Attn: Research & Development Br.

AIR FORCES

41	Office of Technical Services Department of Commerce Washington 25, D. C.	52	U. S. Air Forces Research and Development Div. The Pentagon Washington 25. D. C.

73	Carbide and Carbon Chemicals Div. Central Reports & Information Office P. O. Box P (Y-12) Oak Ridge, Tennessee	82	University of California Radiation Laboratory Information Division Room 128, Building 50 Berkeley, California Attn: Dr. R. K. Wakerling
74	General Electric Company Technical Services Division Technical Information Group P. O. Box 100 Richland, Washington Attn: Miss M. G. Freidank	83	Westinghouse Electric Corp. Atomic Power Division P. O. Box 1468 Pittsburgh 30, Penna. Attn: Librarian
75	Iowa State College P. O. Box 14A, Station A Ames, Iowa Attn: Dr. F. H. Spedding	84	Dr. Geo. Sachs Inst. of Industrial Research Syracuse University East Syracuse 4, N. Y.
76	Knolls Atomic Power Laboratory P. O. Box 1072 Schenectady, New York Attn: Document Librarian	85	Dr. M. Gensamer 91 Columbia University New York, N. Y.
77	Los Alamos Scientific Lab. P. O. Box 1663 Los Alamos, New Mexico Attn: Document Custodian	86	Dr. W. M. Baldwin, Jr. Case Institute of Technology
		87	Dean Elmer Hutchisson Case Institute of Technology
78	U. S. Atomic Energy Commission New York Operations Office P. O. Box 30, Ansonia Station New York 23, N. Y. Attn: Division of Tech. Inf. and Declassification Service	88	Dr. A. R. Troiano Case Institute of Technology
		90	Mr. L. J. Ebert Case Institute of Technology
		91	Mr. E. J. Ripling Case Institute of Technology
79	Oak Ridge National Laboratory P. C. Box P Oak Ridge, Tennessee Attn: Central Files	92	Mr. R. P. Frohmberg Case Institute of Technology
80	Sandia Corporation Sandia Base Classified Document Division Albuquerque, New Mexico Attn: Mr. Dale N. Evans	93	Mr. E. B. Evans Case Institute of Technology
		94	Metals Research Laboratory Case Institute of Technology (File Copy)
81	U. S. Atomic Energy Commission Library Branch, Tech. Inf. Service, ORE P. O. Box E Oak Ridge, Tennessee	95-99	Armed Services Technical Information Agency Documents Service Center Knott Building Dayton 2, Ohio

OVERCOMING RHEOTROPIC EMBRITTLEMENT
BY TORSIONAL PRESTRAIN*

By

I. Rozalsky**

ABSTRACT

A correlation was made of the effects of tensile and torsional prestrain upon the tensile fracture properties of annealed copper, spheroidized SAE 1020 steel and quenched and tempered SAE 1340 steel at various test temperatures.

Evidence of rheotropic behavior was found at subtransition test temperatures for each of the two steels for both tensile and torsional prestrain.

The helical "wolf-ear" tensile fracture obtained subsequent to critical magnitudes of torsional prestrain generally varied in appearance with decreasing supertransition test temperatures and essentially disappeared at subtransition test temperatures.

- - - - - - - - - - - - - - -

INTRODUCTION

In recent attempts to gain insight into the subject of the mechanical behavior of metals, one of the more well-travelled paths through the maze of possible experimental techniques has been the two-step deformation process. Good summaries are available (1)(2)*. A metal is subjected to the first deformation or prestrain under one set of physical conditions and then deformed to fracture under another set of physical conditions. Physical conditions during prestraining may be made different from those during the final test by varying the deformation temperature, stress state, strain rate, etc.

Ripling and Baldwin (3) prestrained quenched and tempered specimens of SAE 1340 steel in tension at supertransition** temperatures where the metal was normally ductile and tested these specimens to fracture in tension at subtransition temperatures where without prestrain the metal would normally exhibit brittle behavior. A plot of the ductility*** retained at the

- - - - - - - - - - - - - - - -

* The numbers in parentheses pertain to the references at the end of this paper.

** The transition temperature for a metal is that usually narrow temperature range within which the mechanical behavior (e.g., ductility) changes from a ductile to a brittle nature. Apparently, only non-face-centered cubic metals exhibit transition temperatures.

*** The criterion of ductility used in this paper was:

$$\mathcal{E} = \ln \frac{\text{Original area}}{\text{Final area}}, \text{ where } \mathcal{E} \text{ is defined as the maximum}$$

natural strain.

subtransition temperature vs. the magnitude of prestrain yielded complex. curves. These curves showed that after an initial decrease in retained ductility for small magnitudes of prestrain, further increases in prestrain increased the retained ductility to a maximum and eventually caused it to pass to zero upon exhaustion of the ductility of the specimen during pre-straining. From their results, Ripling and Baldwin concluded that a part of the ductility deficiency or brittleness at subtransition testing tempera-tures was strain curable or "rheotropic".

Swift (4) prestrained specimens of mild steel in torsion at room temperature and then tested these specimens to fracture in tension at room temperature. With increasing torsional prestrain he observed no appreciable change in the retained tensile ductility until a specimen had been torsionally prestrained to a critical magnitude; whereupon, with increasing torsional prestrain, there was a rapid continuous decrease in ductility for a subsequent tensile test. He also observed a change in fracture appearance from a ductile cup-cone type at subcritical magnitudes of prestrain to a brittle, helical "wolf-ear" type at supercritical magni-tudes of torsional prestrain.

Fig. 1(a-e) indicates schematically the tensile deformation behavior for metals subsequent to various types of prestrain. The ordinate axis in-dicates the retained tensile ductility; whereas, the abscissa axis indicates the magnitude of prestrain. Terminal points of the curve on the abscissa axis or the ordinate axis indicate single deformation processes where the

ductility is exhausted exclusively under either prestraining or testing conditions respectively.

Fig. 1 (a) shows the deformation behavior for simple tensile prestrain when the prestrain temperature and test temperature are identical for (a) metals (FCC) which exhibit no transition temperature, or (b) at supertransition test temperatures for metals which do exhibit a transition temperature. The curve is a straight line of 45 degree slope.

Fig. 1(b) shows the deformation behavior for torsional prestrain under the conditions stated above for Fig. 1(a). Here the relationship is not as simple as that given above. One should realize, however, that the strain states for tensile and torsional prestrain differ from each other as do their respective stress states. With increasing torsional prestrain, the retained tensile ductility first decreases at a rather slow and essentially linear rate (the subcritical branch of the curve) until a critical prestrain is reached; whereupon, with further increase in prestrain, there is a rapid decrease in the retained ductility (the supercritical branch of the curve). The introduction of the critical magnitude of torsional prestrain into the test specimen is accompanied by a change in the tensile fracture appearance from one which for subcritical magnitudes of torsional prestrain is of a "cup-cone" type to one of a helical type, Swift's (4) so called "wolf-ear" fracture. Finally, with further prestrain the curve becomes approximately horizontal (the terminal branch of the curve) and remains so up to the point of fracture in torsional prestrain (exhaustion

of the ductility of the metal in torsion). The helical type of fracture

continues to persist in the tension test up to this point. This overall

type of curve has been obtained in several investigations for a number

of ductile, relatively pure metals and single phase alloys (5)(6).

Fig. 1(c) shows, for metals exhibiting a transition temperature,

the effect of prestraining in tension at a supertransition temperature,

T_1, upon the retained tensile ductility at another supertransition temper-

ature, T_2, where $T_1 > T_2$. Here $\Delta \xi_1$, indicates the difference between

the ductilities of the metal at the given temperatures. This type of be-

havior was obtained for specimens of quenched and tempered (above $800^\circ F$)

SAE 1340 steel prestrained in tension at room temperature and then tested

in tension at $-321^\circ F$ (3). A similar type of curve was obtained for 24S-T4

aluminum (no transition temperature) by prestraining at room temperature

and testing at $-321^\circ F$ (7).

No analogous investigation has as yet been conducted to determine

the deformation behavior for torsional prestrain at different supertransition

prestrain and test temperatures when the prestrain temperature is higher

than the testing temperature.

Prestraining in tension at a supertransition temperature and testing

in tension at a subtransition temperature yields the relatively complex

curve illustrated in Fig. 1d. Upon extrapolating the stable portion of the

curve to the ordinate axis, Ripling and Baldwin (3) concluded that the low

temperature ductility deficiency ($\Delta \xi_1 + \Delta \xi_2$) of quenched and tempered

SAE 1340 steel was in part ($\Delta\varepsilon_2$) rheotropic, i.e., strain curable.

Ripling and Baldwin (8) found that prestraining SAE 1340 steel specimens in compression at supertransition temperatures was also capable of restoring part of the ductility normally denied the steel at subtransition test temperatures, in fact, at much lower magnitudes of prestrain than by prestrain in tension (see Fig. 1e). What would the effect of torsional prestrain be under similar conditions?

Fig. 2a previously presented by Ripling and Baldwin (8) shows that after an initial increase in the retained ductility for small compressive prestrains (rheotropic recovery) there is a rapid ductility decrease with increased magnitudes of prestrain. Was this ductility drop-off due to "microcracks", as was proposed by Backhofen et al (5) (6) for the ductility decrease for torsional prestrain? The magnitude of prestrain at which the rapid ductility drop-off takes place recedes to smaller and smaller values with decreasing temperature, see Fig. 2a. Would the ductility drop-off obtained by Swift (4) subsequent to torsional prestrain similarly recede under analogous conditions?

But the precompression by Liu (7) of 24S-T4 aluminum, a ductile face centered cubic metal, showed (see Fig. 2b) no ductility drop-off as severe as that for steel. Does this mean 24S-T4 aluminum is insensitive to microcracks? On the other hand, copper (also a ductile facecentered cubic metal) showed a ductility drop-off after pre-torsion at a magnitude of prestrain where it was claimed cracks did occur (5).

The objective of the present investigation was a correlation of the effects of tensile and torsional prestrain upon the tensile fracture properties (retained ductility and fracture stress) of several metals at various testing temperatures. The metals chosen were copper, crystallizing in the facecentered cubic system and, concomitantly, showing no transition temperature, and two steels, a plain carbon SAE 1020 steel and a low alloy SAE 1340 steel. Both of these steels are body centered cubic and exhibit a transition temperature.

MATERIAL AND PROCEDURE

The materials used in this investigation were (a) annealed electro-lytic tough pitch copper, (b) plain carbon SAE 1020 steel in the spher-oidized condition, and (c) low SAE 1340 steel in the water quenched and tempered (600°F) condition*.

Torsional prestrain specimens of the type shown in Fig. 3b were twisted various amounts at a strain rate of approximately 120 degrees per minute. The plastic shear strain, γ, at the surface of the reduced section of a twisted torsion specimen was calculated from the relation:

$$\gamma = \frac{R\Theta}{L},$$

where

γ = plastic surface shear strain (circular bar)
R = radius of bar
Θ = total twist in radians
L = length of bar over which twisting occurs.

Although some doubt has been expressed concerning the validity of the above expression for large magnitudes of strain (9), the author con-sidered the use of the above simple equation adequate for this investiga-tion.

After the desired magnitude of torsional prestrain had been effected, a tensile test specimen of the type shown in Fig. 3a was machined from the

- - - - - - - - - - - - - - - - -

* Details of the heat treating, prestraining and testing procedures used in the investigation are found in the Appendix.

center of the reduced section of the torsion specimen. Because of the
linear strain gradient with respect to the radius of the twisted bar
(γ = O at the center) the magnitude of shear strain at the surface of
the reduced section of the tensile test specimen was readily calculated.

Tensile prestrain was obtained on specimens of the type shown
in Fig. 3a. It was not considered necessary to remachine specimens
after tensile prestrain. All tensile prestrains and tensile tests were
made on a hydraulic tensile testing machine with a head speed of 0.05
inch per minute.

RESULTS AND DISCUSSION

Retained Tensile Ductility

Copper

In order to establish the simplest mode of tensile deformation behavior subsequent to tensile or torsional prestrain* without the complication of transition temperature, the initial tests were conducted with soft ductile copper. The results are shown in Fig. 4. The tensile ductility for zero prestrain at a test temperature of -321°F was approximately equal to that at a test temperature of +75°F. The linear type curves described in the Introduction (Figs. 1a and 1c) for retained tensile ductility versus tensile prestrain were obtained for copper in Fig. 4.

The curves for retained tensile ductility, $\mathcal{E}_f$,** versus torsional prestrain at test temperatures of +75°F and -321°F are quite similar to one another. For each given test temperature the critical shear strain required to initiate a helical "wolf-ear" tensile fracture was approximately $\gamma = 1.6$. The sub-critical branch of the curve extended from $\gamma = 0.0$ to $\gamma = 1.6$: the supercritical branch of the curve extended from $\gamma = 1.6$ to approximately $\gamma = 2.0$ and the terminal branch extended from approximately $\gamma = 2.0$ to approximately $\gamma = 2.5$

- - - - - - - - - - - - - - - -

* All of the tensile and torsional prestraining operations in this investigation were performed at room temperature (+75°F).

** $\mathcal{E}_f = \ln \dfrac{\text{Area After Prestrain}}{\text{Final Area}}$

It should be noted that the maximum torsional prestrain obtainable (γ = 2.5) for copper at +75°F in this investigation does not imply exhaustion of the ductility for this material by this magnitude of torsional strain at this temperature for fracture during twisting occurred not in the reduced section but in the shoulder fillet of the torsion specimen (see Fig. 3b) where the stress concentration factor was of the magnitude K = 1.3 (10).

Helical or "Wolf-Ear" Fracture

Photographs of tensile fractures at test temperatures of +75°F and -321°F for specimens of the annealed copper torsionally prestrained to various magnitudes of surface shear strain, γ, are shown in Fig. 5. With increasing torsional prestrain at both test temperatures, the tensile fracture was of the ductile cup-cone type until the magnitude of surface shear strain γ = 1.60 was attained. At this value, the first propensity towards the helical type of fracture became evident. This effect became more pronounced with increased magnitudes of torsional prestrain as is evidenced in Fig. 5.

The fracture surfaces of the copper tensile specimens torsionally prestrained to critical (γ = 1.60) or supercritical (γ>1.60) magnitudes of surface shear strain are essentially crystalline or brittle in nature, as contrasted to the ductile or silky type of fracture surface at the lip of the cup of a tensile specimen exhibiting a cup-cone type of fracture.

Upon comparison of the tensile fractures in Fig. 5, it is observed that specimens torsionally prestrained to equivalent amounts but tested

in tension at different temperatures (+ 75°F and -321°F) exhibit similar fracture appearances be those fractures of the cup-cone type or helical "wolf-ear" type. This observation should be tempered by the consideration of almost identical tensile ductilities at zero prestrain for copper at test temperatures of + 75°F and -321°F. Whether the above similarities in fracture appearance would exist for a metal where different tensile ductilities at zero prestrain are obtained at different test temperatures is at this point not known.

Stimulated by Griffith's (11) microcrack theory in which he considered stress concentrations at the edges of submicroscopic cracks as the cause of the lowering of the cohesive strength in brittle materials from a high theoretical value, a number of possible explanations of the helical tensile fractures for normally ductile metals subsequent to pre-torsion have arisen.

Swift (4) deduced that the helical "wolf-ear" tensile fracture was a manifestation of a shear type failure because of the delineation of the plane of maximum shear in tension (45 degrees with respect to the tensile axis) by the fracture surface. He postulated that the effect of the torsional prestrain was to lower the shear stress required to produce a shear failure in tension rather than a conventional normal tensile fracture.

Gensamer (12) preferred to consider the "wolf-ear" fracture as a normal fracture by postulating that pre-torsion had reduced the normal stress required to cause fracture on a 45 degree plane so that the specimen

exhibited a preference to fracture on a plane subjected to the maximum normal stress in torsion rather than on one subjected to the maximum normal stress in tension.

Zener and Hollomon (13) extended Griffith's theory by eliminating the assumption that cracks need be present in the metal prior to deformation and considered such possible sources of crack formation during deformation as the fracture of brittle constituents or weak interphases. They concluded that microcracks are responsible for the helical type of fracture.

Backofen et al (5) (6) have considered the helical type of fracture after pre-torsion from the viewpoint of aligned microcracks. They postulated that after the severe reduction of a metal by rolling, forging, etc. into a bar, all the cracks will be aligned parallel to the direction of working. During the process of twisting a specimen parallel to this direction, they considered that the cracks will be realigned at an angle ϕ with respect to the specimen axis, so that the torsional shear strain at the surface, γ, will be

$$\gamma = \tan \phi = \frac{R\dot{\Theta}}{L}$$

where R is the distance of the crack from the specimen axis, and $\frac{\Theta}{L}$ is the angle of twist in radians per unit length.

Effective Strain

In Fig. 4, for both test temperatures ($+75^\circ$F and -321°F) the super-

critical branch of each torsional prestrain curve extrapolated to the abscissa axis to a value of torsional shear strain of approximately $\gamma = 2.48$. On the other hand each of the retained tensile ductility curves ($+75^{\circ}F$ and $-321^{\circ}F$) for tensile prestrain possessed a terminal point on the abscissa axis equal to $\mathcal{E}_p = 1.43$ (the tensile ductility of the copper at zero prestrain at $+75^{\circ}F$). It seemed reasonable, then, that the first step in the attempt to correlate the effects of tensile and torsional prestrain upon the retained tensile ductility involved the further consideration of these values ($\mathcal{E}_p = 1.43$ and $\gamma = 2.48$).

In order to effect the above correlation, consideration was given to the generalized or effective stress-strain relations (14)

$$\bar{\sigma} = \sqrt{1/2 \left[(\sigma_1 - \sigma_2)^2 + (\sigma_2 - \sigma_3)^2 + (\sigma_3 - \sigma_1)^2 \right]}$$

$$\bar{\mathcal{E}} = \sqrt{2/3 (\mathcal{E}_1^2 + \mathcal{E}_2^2 + \mathcal{E}_3^2)}$$

where σ_1, σ_2 and σ_3 are the true principal stresses; $\mathcal{E}_1$, $\mathcal{E}_2$, and $\mathcal{E}_3$ are the true principal strains; $\bar{\sigma}$ is the effective stress and $\bar{\mathcal{E}}$ is the effective strain.

From the above equation for strain:

$$\bar{\mathcal{E}}_p = \mathcal{E}_p \text{ for tensile prestrain,}$$

$$\bar{\mathcal{E}}_p = \gamma \text{ for torsional prestrain,}$$

$$\bar{\mathcal{E}}_f = \mathcal{E}_f \text{ for retained tensile ductility.}$$

Justification for employing this form of effective strain is based on

the results of Jackson (15) and Lankford (16) who showed that if pre-
strain under a stress state different from tension was plotted in terms
of effective strain, the composite stress strain curve coincided with
one obta.ned for simple tension alone.

Fig. 6 shows such a plot in terms of effective prestrain for copper
for test temperatures of +75°F and -321°F. At each temperature the
supercritical branch (neglecting the terminal branch) of the curve for
torsional prestrain extrapolates to the same value of effective prestrain
as the terminal point on the abscissa axis for the tensile prestrain curve.

Several curves showing the effect of torsional prestrain at room
temperature upon the retained tensile ductility at room temperature (in
terms of reduction in area) have been taken from the literature (4)(5)(17)
and replotted in terms of effective prestrain and effective retained tensile
ductility in Fig. 7.

Although for both the electrolytic tough pitch copper (5) and the
annealed commercial SAE 4340 steel (17) the supercritical branch of the
curve extrapolates to the same value of effective prestrain as the tensile
ductility at zero prestrain of the respective metal, this is not the case
for the annealed mild steel (4). No explanation can be made at this time
for the non-conformity of this latter steel.

In the present investigation of copper, the critical magnitude of
torsional prestrain necessary to cause the rapid decrease in retained
tensile ductility and the helical type tensile fracture is independent of test

temperature. This effect is shown to greater advantage in Fig. 8. Here the ratio of the retained ductility to the ductility at zero prestrain for each test temperature is plotted versus the ratio of the effective (torsional or tensile) prestrain at $+75^{O}F$ to the fracture ductility at $+75^{O}F$.

These results may be compared with those in Fig. 2b for the pre-compression of 24S-T4 aluminum, also a face-centered cubic alloy. Although the shape of the curves for either copper or aluminum is essentially independent of test temperature, the aluminum does not, in contrast to the copper, show a rapid drop-off in retained tensile ductility at any magnitude of prestrain.

SAE 1020 Steel

Transition Temperature

Tensile test specimens of spheroidized SAE 1020 steel were tested in tension at various temperatures in the range $+75^{O}F$ to $-321^{O}F$. The experimental curves for retained tensile ductility, ξ_f, versus test temperature and for tensile fracture stress, s_f^*, versus test temperature are shown in Fig. 9.

Unfortunately, there is no narrow temperature range on the retained ductility curve which defines the transition temperature. However, by examination of the fractured specimens, it was possible by observations

- - - - - - - - - - - - - - - -

* $s_f = \dfrac{\text{Load at Fracture}}{\text{Fracture Area}}$

similar to those made by Eldin and Collins (18) on a mild steel to deter-
mine the highest test temperature at which completely brittle fracture
occurred in simple tension.

At test temperatures of $-260^\circ F$ and below, the fracture surfaces
of the tensile specimens were entirely brittle and crystalline in appear-
ance. However, at a test temperature of $-240^\circ F$, the fracture surface
contained at its center a dark, non-crystalline, fibrous circle of approxi-
mately 2-3 millimeters in diameter, the remainder of the fracture surface
retaining the crystalline appearance characteristic of lower test tempera-
ture fractures. With increasing test temperature, the size of this dark dot
increased at the expense of the brittle portion of the fracture surface until
at a test temperature of $-120^\circ F$, the black circle covered the whole fracture
surface, i.e., the fracture was now entirely of the ductile cup-cone type.
It was concluded that any test temperature at which there was visual evi-
dence of a fibrous portion in the fracture surface was above the transition
temperature of the steel. Hence, the transition temperature for the SAE
1020 steel was estimated to be $-250^\circ F$.

It is also interesting to note that the tensile fracture stress attains
its maximum value at this test temperature.

Effect of Tensile or Torsional Prestrain at Supertransition Test Temperatures

After tensile or torsional prestrain of the SAE 1020 steel at $+75^\circ F$,
subsequent tensile tests were performed at three different supertransition

temperatures ($+75^\circ$F, -110°F and -200°F).

The curves for retained tensile ductility ($\mathcal{E}_f$) versus prestrain in tension ($\mathcal{E}_p$) or torsion (γ) at the three supertransition test temperatures are shown in Fig. 10. As expected, the retained ductility versus tensile prestrain curve for each of these test temperatures is a straight line. The terminal point on the abscissa axis is equal to the tensile ductility ($\mathcal{E}_p = 1.26$) at the prestrain temperature; the terminal point on the ordinate axis is equal to the tensile ductility at the test temperature, i.e.,

$\mathcal{E}_f = 1.26$ at $+75^\circ$F; $\mathcal{E}_f = 1.12$ at -110°F; and $\mathcal{E}_f = 0.92$ at -200°F.

At the supertransition test temperatures the curves for retained tensile ductility versus torsional prestrain, Fig. 10, are similar to those obtained for the copper (see Fig. 4) used in this investigation. However, for the SAE 1020 steel, even at a test temperature of $+75^\circ$F, there is no terminal branch to the curve as for copper. This factor may be due to a lack of sufficient ductility in torsion, i.e., the maximum surface shear strain obtained experimentally by torsional prestrain for the steel was approximately $\gamma = 1.9$. The approximately linear subcritical branch of each curve ($+75^\circ$F, -110°F and -200°F) extends to an approximate value of $\gamma = 1.6$ to 1.7. Also as the test temperature is lowered, the subcritical branch of each curve becomes flatter. The supercritical branch of the torsional prestrain curve for each of the different supertransition test temperatures extrapolates to the same value $\gamma = 2.17$ on the abscissa (torsional prestrain) axis.

Helical ''Wolf-Ear'' Fracture

Fig. 11 shows fractures of specimens of SAE 1020 steel torsionally prestrained at $+75^{\circ}$F to various magnitudes of surface shear strain and subsequently tested in tension at the supertransition temperatures of $+75^{\circ}$F, -110°F, and -200°F.

The photographs in column A of Fig. 11 show the change in fracture appearance with test temperature at zero prestrain ($\gamma = 0.00$). Although the fractures for test temperatures of $+75^{\circ}$F and -110°F are of the ductile cup-cone type, the fracture at -200°F tends to be more brittle in nature and exhibits the small dark fibrous circle at its center as previously described. These photographs are the prototypes of fractures for tensile specimens torsionally prestrained to subcritical magnitudes of surface shear strain.

The photographs in column C of Fig. 11 show fractures obtained for tensile specimens torsionally prestrained to supercritical magnitudes of surface shear strain. It is noted that with decreasing test temperature, there is an increased degeneracy in the appearance of the helical ''wolf-ear'' fracture. This increased deterioration with decreasing test temperature is detectable with somewhat less ease for the fractured tensile test specimens torsionally prestrained to critical magnitudes ($\gamma = 1.6$ to $\gamma = 1.7$), as shown in column B of Fig. 11.

At the test temperature of -200°F, it is interesting to note that the dark fibrous dot at the center of the fractured specimens twisted to

subcritical magnitudes of shear strain is no longer evident, see Fig. 11, when a critical (γ = 1.60) or supercritical (γ = 1.86 magnitude of surface shear strain is introduced into the specimen, prior to testing in tension. If the fibrous dot indicates that some semblance of ductility is present in tension at -200°F for zero torsional prestrain, then its absence after a critical or supercritical magnitude of torsional prestrain indicates that the presence of a helical type of fracture is associated with a decrease in ductility.

The wolf-ear or helical type tensile fractures obtained at different test temperatures subsequent to equal magnitudes of supercritical torsional prestrain are quite similar when the tensile ductilities at zero prestrain are approximately equal (see Fig. 5 for copper). But they are quite different when the tensile ductilities at zero prestrain vary, i.e., they degenerate in appearance with decreasing test temperature, see Fig. 11 for SAE 1020 steel.

For any metal, per se, the degree of manifestation and appearance of the helical "wolf-ear" fracture itself seem to be functions of the tensile ductility at zero prestrain (γ = 0.0) for that metal. Also, when any indication of low temperature brittleness is detectable in the appearance of the tensile fracture surface for zero prestrain, there is a pronounced tendency for degeneracy in the appearance of the "wolf-ear" tensile fracture after a critical or supercritical magnitude of torsional prestrain, see Fig. 11 (test temperature -200°F).

Effect of Tensile and Torsional Prestrain at Subtransition Test Temperatures.

The curves for SAE 1020 steel for retained tensile ductility (ε_f) versus prestrain in tension (ε_p) or torsion (γ) at the three subtransition test temperatures (-280°F, -300°F and -321°F) are shown in Fig. 12.

For tensile prestrain, the curves are of the type obtained by Ripling and Baldwin (3) for an annealed steel. The basic three branches - the metastable, the transition and the stable branches - were obtained for each curve at each of the three subtransition test temperatures. With decreasing test temperature the amount of tensile prestrain necessary to attain a minimum in the curve decreases and the prestrain necessary to attain a maximum in the curve increases.

The stable branch of the tensile prestrain curve at each subtransition test temperature extrapolates to the ordinate axis to a value of retained ductility which falls on the curve obtained by extrapolating the supertransition part of the retained tensile ductility versus test temperature curve in Fig. 9. For any subtransition test temperature, the difference in retained ductility between the extrapolated curve and the experimental curve denotes that part of the low temperature ductility deficiency which is rheotropic in nature.

The curves for retained tensile ductility versus torsional prestrain at test temperatures of -280°F and -300°F resemble those for tensile prestrain in that each is composed of the three usual parts, i.e., the

metastable, transition and stable branches. Again, with decreasing test temperature the amount of torsional prestrain necessary to attain a minimum in the curve decreases (including the -321°F test temperature), and the torsional prestrain necessary to attain a maximum increases.

It was not possible to obtain data for specimens prestrained in torsion to surface shear strains greater than 1.45 and tested in tension at -321°F because all such specimens fractured during the tension test at points along the axis of the tensile specimen which were removed from the minimum section. However, had such tests been possible, it is expected (after examination of the other curves) that a maximum would have occurred in the retained ductility versus torsional prestrain curve at approximately $\gamma = 1.9$.

Fracture Appearance at Subtransition Test Temperatures

All of the tensile fractures obtained after torsional prestrain at test temperatures of -280°F, -300°F and -321°F were of the brittle crystalline type (no fibrous dark dot at the center of the fracture surface).

For a test temperature of -280°F helical markings were present on the external surface of fractured tensile test specimens subsequent to a torsional surface shear strain greater than or equal to 1.65, but no wolf-ear fractures, per se, were observed. Data for these values fall well along the stable portion of the curve, see Fig. 12.

For a test temperature of -300°F these helical markings were obtained on fractured tensile test specimens torsionally prestrained to a

surface shear strain greater than or equal to 1.65. In fact, the maximum in the retained tensile ductility versus torsional prestrain curve falls at this magnitude of torsional prestrain ($\gamma = 1.55$).

But for a test temperature of $-321^\circ F$ not only no helical "wolf-ear" fractures but also no helical surface markings were observed for any of the fractured tensile test specimens previously prestrained in torsion up to the experimental limit $\gamma = 1.45$. Upon consideration of the surface shear strain gradient along the axis of the tensile test specimen, see Fig. 3, after torsional prestrain, the reduction in section size at the center (of length) of the tensile test specimen may have been of insufficient magnitude to prevent the specimen from fracturing where it willed along the specimen axis at extremely low test temperatures.

Retained Tensile Ductility Versus Effective Prestrain

Fig. 13 shows curves for SAE 1020 steel of retained tensile ductility (effective) versus effective prestrain ($\bar{\varepsilon}_p = \varepsilon_p$) for tensile prestrain ($\bar{\varepsilon}_p = \gamma/\sqrt{3}$ for torsional prestrain) at the three subtransition and three supertransition test temperatures used in this investigation. Since $\bar{\varepsilon}_p = \varepsilon_p$, the curves for tensile prestrain are the same as those shown in Figs. 10 and 12.

The torsional prestrain curves in Fig. 13 are similar to those shown in Figs. 10 and 12, but are essentially compressed along the abscissa axis for $\bar{\varepsilon}_p = \gamma/\sqrt{3}$. On the basis of effective prestrain, the terminal point on the abscissa axis for the stable branch of the tensile prestrain curve is

identical to the terminal point on the abscissa axis for the extrapolated

stable branch of the torsional prestrain curve at each of the test temper-

atures. However, although the curves for tensile and torsional prestrain

at the subtransition temperatures are somewhat similar in shape (except

for -321°F), the maxima and minima in the curves obtained for each

mode of prestrain do not correspond in magnitude of effective prestrain,

nor do the retained tensile ductilities obtained under these conditions

correspond in magnitude.

Rheotropic Embrittlement

For test temperatures of -280°F and -300°F (see Fig. 12) the

stable branches of the retained tensile ductility versus torsional pre-

strain curves both extrapolate to values of approximately $\mathcal{E}_f$ = 1.5 on

the ordinate (retained tensile ductility) axis. This extrapolated value is

of greater magnitude than the tensile ductility of the SAE 1020 steel at

+75°F. It is possible that the slope of the stable branch of the ductility

versus torsional prestrain curve at test temperatures of -280°F and

-300°F may have been sufficiently influenced by the steep slope of the

supercritical branch of the ductility (+75°F) versus torsional prestrain

curve, see Fig. 10, in such a manner as to cause a difference between the

extrapolated ductility values for the stable branches of the ductility versus

tensile prestrain and ductility versus torsional prestrain curves for each

of the above test temperatures.

The stable branch of each curve (see Fig. 12) at the given test

temperatures extrapolates to γ = 2.17 on the abscissa (torsional pre-strain) axis. This value is identical to the extrapolated value of the supercritical branch of the retained tensile ductility versus torsional prestrain curves for the spheroidized SAE 1020 steel at the super-transition test temperatures, +75°F, -110°F, and -200°F, in Fig. 10.

For subtransition test temperatures, matching up the terminal points by means of effective prestrain (see Fig. 13) for each test temperature does not imply point for point coincidence of the curves for different modes of prestrain. It appears that the positions and magnitudes of the maxima and minima are at least in part a function of the prestrain stress state.

This lack of point for point coincidence is further emphasized in Fig. 14 where like for copper, see Fig. 8, the ratio of the retained tensile ductility to the ductility at zero prestrain* for each test temperature is plotted versus the ratio of the effective prestrain to the fracture ductility at +75°F. For this reduced or normalized type of plot at each test temperature there is matching only of the terminal points for the tensile and torsional prestrain curves.

A similar reduced type of plot for tests at room temperature is shown in Fig. 15 for the copper and SAE 1020 steel used in this investigation, Fields' (17) SAE 4340 steel, Swift's (4) mild steel and Backofen's (5)

- - - - - - - - - - - - - - -

* In the absence of rheotropic embrittlement for subtransition test temperatures.

tough pitch copper. With the inexplicable exception of the mild steel the supercritical branch of the torsional prestrain curve for each of the above metals extrapolates to the abscissa axis to the same value (1.0 on the reduced plot) as the terminal point on the abscissa axis for the tensile prestrain curve.

The curves in Fig. 8 for copper (FCC) and in Fig. 14 for SAE 1020 steel (BCC) are combined in Fig. 16. Certain similarities between curves are evident. The torsional prestrain curves for the copper and for the SAE 1020 steel at supertransition test temperatures are relatively alike in shape.

For the steel at the subtransition test temperatures of -280°F and -300°F, each curve for tensile or torsional prestrain consists of the requisite three branches: metastable, transition and stable.

For both tensile and torsional prestrain at subtransition test temperatures, the magnitude of reduced prestrain necessary to attain a minimum in the curve decreases with decreasing test temperature; whereas, the magnitude of reduced prestrain necessary to attain a maximum in the curve increases with decreasing test temperature.

The slope of the stable branch of each curve (-280°F and -300°F) for torsional prestrain is intermediate between the slope (45°) of the stable branch of each curve (-280°F and -300°F) for tensile prestrain and the very steep slope of the supercritical branch of the curve obtained for a supertransition test temperature (+75°F, -110°F, or -200°F).

As previously mentioned, this factor may serve as a possible source of explanation for the difference between the extrapolated ductility values for the stable branches of the tensile prestrain and torsional prestrain curves for each of the subtransition test temperatures for the SAE 1020 steel (see Fig. 12).

An examination of the photographs in Fig. 11 shows the elimination of the "wolf-ear" tensile fracture for torsional prestrain at subtransition test temperatures. It appears that the type of tensile fracture obtained at any test temperature subsequent to critical or supercritical magnitudes of surface shear strain is a manifestation of the competitive effort between (a) the propensity towards a "wolf-ear" helical type fracture and (b) the tensile fracture normally obtained for the non-prestrained metal at the given test temperature.

Thus at high supertransition test temperatures, the tensile ductility at zero prestrain is high and the "wolf-ear" fracture manifests itself in its complete form. At low subtransition test temperatures the tensile ductility at zero prestrain is low and hence the low temperature enbrittling effect overshadows the tendency towards a "wolf-ear" fracture - the only manifestation of "wolf-ear" fracture propensity consists of helical surface markings on the fractured tensile specimen. At any intermediate test temperature, the final fracture appearance would also be a compromise between these extremes: (a) the helical "wolf-ear" fracture, important at high test temperatures and (b) the fracture due to low temperature

embrittlement, characteristic of course only at low test temperatures.
There are differences between these two types of fracture, but the
appearance of each type connotes the presence of an embrittlement
mechanism.

SAE 1340 Steel

Effect of Tempering Temperature

Fig. 17 shows curves for retained tensile ductility and tensile
fracture stress versus tempering temperature for quenched and tempered
SAE 1340 steel tested at -321°F. A minimum in ductility occurs at a
tempering temperature of 500°F. The maximum in ductility at a temper-
ing temperature of 400°F has been found by Ripling and Baldwin (3) for
SAE 1340 steel, but the large magnitude of this maximum obtained in this
investigation is somewhat unexpected.

The curve for tensile fracture stress versus tempering temperature
shows (as expected from the retained ductility versus tempering tempera-
ture curve) a maximum and minimum at tempering temperatures of 400°F
and 500°F respectively. In addition, there is another slight maximum in
the fracture stress at a tempering temperature of 700°F.

Fig. 18 shows the effect of test temperature upon the retained tensile
ductility and fracture stress of SAE 1340 steel quenched and tempered at
600°F. The transition temperature was estimated to be approximately
-240°F.

Effects of Tensile and Torsional Prestrain

Fig. 19 shows the effect of tensile and torsional prestrain upon the retained ductility for two supertransition test temperatures, + 75°F and -200°F, and one subtransition test temperature, -321°F, for quenched and tempered (600°F) SAE 1340 steel.

For each of the supertransition test temperatures, the retained tensile ductility versus tensile prestrain curve is a straight line. The terminal point on the abscissa axis is equal to the tensile ductility at the prestrain temperature; the terminal point on the ordinate axis is equal to the tensile ductility at the test temperature.

The maximum amount of shear strain experimentally obtainable on the surface of torsionally prestrained tensile test specimens for the quenched and tempered SAE 1340 steel was quite small in comparison to that possible for the spheroidized SAE 1020 steel.

At a test temperature of + 75°F the retained tensile ductility versus torsional prestrain curve is linear in nature up to the maximum magnitude of torsional prestrain experimentally possible, but at a test temperature of -200°F the curve is linear for small magnitudes of torsional prestrains and then drops off rapidly for larger prestrains.

In the results for copper and SAE 1020 steel (at supertransition test temperatures) this rapid loss of tensile ductility was associated with the appearance of a helical or "wolf-ear" tensile fracture at supercritical magnitudes of torsional prestrain. However, for the SAE 1340 steel, no

helical type tensile fractures were obtained concomitant with this rapid ductility decrease.

A comparison of the curves showing the effects of tensile and torsional prestrain on the retained tensile ductility at -321°F reveals both similarities and differences. For both types of prestrain, each curve reveals a metastable, a transition and a stable branch.

The stable portion of the retained ductility (-321°F) versus tensile prestrain curve, Fig. 19, extrapolates to a ductility value on the ordinate axis equal in magnitude to that obtained for an extrapolation of the super-transition portion of the retained ductility versus test temperature curve, Fig. 18. At a test temperature of -321°F, the ductility difference between the extrapolated and experimental curve is equivalent to that part of the low temperature ductility deficiency which is rheotropic in nature.

Although a large number of tensile test specimens of SAE 1340 steel torsionally prestrained to surface shear strains greater than 0.20 were tested in tension at -321°F, all but one, $\gamma = 0.26$, fractured at points removed from the center of the reduced section of the tensile test specimen. Therefore, because of the variation of surface shear strain along the axis of the tensile test specimen, the slope of the stable branch of the retained tensile ductility versus torsional prestrain curve is predicated upon but one test specimen. Even assuming that the slope of the stable branch of this curve is approximately correct, the slope is too steep to permit an accurate extrapolation to the ordinate axis.

No helical type tensile fracture was observed for the quenched and tempered SAE 1340 steel for any magnitude of torsional prestrain obtainable in this investigation.

The maximum magnitude of torsional prestrain attainable prior to fracture in torsion for the quenched and tempered ($600^{\circ}F$) SAE 1340 steel was exceedingly limited in comparison to that obtained for either the annealed copper or the spheroidized SAE 1020 steel.

The possibility of directionality for this steel was considered, and a few tests were run on fully annealed steel. Fig. 20 shows the effect of torsional prestrain upon the retained ductility and fracture stress for the annealed steel. Even in the annealed condition, the maximum magnitude of torsional prestrain possible was still quite limited and insufficient to obtain a helical "wolf-ear" type of tensile fracture. However, the shape of the curve for retained tensile ductility versus torsional prestrain is similar to that for the supercritical branch of that for either annealed copper. See Fig. 4, or SAE 1020 steel at a supertransition test temperature, see Fig. 10.

Retained Tensile Ductility versus Effective Prestrain

Fig. 21 shows the curves for retained tensile ductility versus torsional and tensile prestrain in terms of effective prestrain for test temperatures of $+75^{\circ}F$, $-200^{\circ}F$ and $-321^{\circ}F$.

At a test temperature of $-321^{\circ}F$, the metastable branches of the ductility curves for both types of prestrain are approximately coincident; however, there are again distinct differences in position and magnitude for the maxima

and minima for the curves as was also evidenced for the SAE 1020 steel

tested at subtransition test temperatures.

Tensile Fracture Stress

Although the majority of emphasis in this investigation was placed

upon a correlation of the effects of tensile and torsional prestrain upon

the retained tensile ductility of copper, SAE 1020 steel and SAE 1340 steel,

some consideration was given to a comparison of the effects of tensile and

torsional prestrain upon the other tensile fracture property, the tensile

fracture stress.

Copper

Fig. 22 shows the effects of tensile and torsional prestrain upon the

tensile fracture stress for annealed copper at test temperatures of $+75^{\circ}F$

and $-321^{\circ}F$.

For a test temperature of $+75^{\circ}F$, the fracture stress remains constant

with increasing tensile prestrain. When the prestrain stress state is changed

to torsion, the fracture stress curve becomes more complex. With increasing

torsional prestrain, the fracture stress decreases very slightly for subcritical

magnitudes of torsional prestrain. At supercritical magnitudes of torsional

shear strain, the presence of the helical "wolf-ear" fracture is accompanied

by a rapid decrease in fracture stress (4) until a torsional prestrain equal in

magnitude to the beginning of the terminal branch of the retained ductility

versus torsional prestrain curve is reached, see Fig. 4. Thereupon the fracture

stress continues to increase with increasing torsional prestrain.

At a test temperature of -321°F, the fracture stress curves for tensile and torsional prestrain are quite similar to those described above for a test temperature of +75°F, except that there is no minimum exhibited in the fracture stress versus torsional prestrain curve.

It is evident that not only is the attainment of the helical "wolf-ear" tensile fracture accompanied by a decrease in retained tensile ductility but also by a rapid decrease in tensile fracture stress.

SAE 1020 Steel

Figs. 23 and 24 show the effects of tensile and torsional prestrain upon the tensile fracture stress for SAE 1020 steel at the three super-transition test temperatures and the three subtransition test temperatures respectively.

At +75°F and -110°F, the tensile fracture stress remains constant with increasing tensile prestrain. With increasing torsional prestrain at both of these test temperatures, the fracture stress increases slightly until at approximately the critical magnitude of torsional prestrain the fracture stress decreases rapidly with increasing prestrain.

At a test temperature of -200°F, increasing tensile prestrain causes a slight linear increase in the tensile fracture stress. However, for increasing torsional prestrain the fracture stress at -200°F remains constant for an interval of prestrain, then attains a maximum value and finally continues to decrease with increasing torsional prestrain. The appearance of the helical

"wolf-ear" fracture at this test temperature does not cause any change in shape of the fracture stress versus torsional prestrain curve.

The tensile fracture stress versus tensile prestrain curves at the test temperatures of -280°F, -300°F, and -321°F are all quite similar, see Fig. 24. With increasing tensile prestrain, the fracture stress increases rather rapidly, reaches a maximum value and then starts to descend. The curve for a test temperature of -280°F is quite similar in shape to that at -200°F, even though, from a point of view of tensile ductility, -200°F is considered to be a supertransition temperature and -280°F a subtransition temperature.

At a test temperature of -300°F, the fracture stress remains constant for an interval of torsional prestrain and then continually increases in a linear manner with increasing torsional prestrain.

But at a test temperature of -321°F the fracture stress increases immediately with increasing torsional prestrain, and then with further increased prestrain the curve eventually flattens out.

It should be noted from Figs. 23 and 24 that the appearance of the helical "wolf-ear" fracture assumes less importance with decreasing test temperature in influencing the shape of the tensile fracture stress versus torsional prestrain curve at a given test temperature.

SAE 1340 Steel

Fig. 25 shows the effect of tensile and torsional prestrain upon the tensile fracture stress at the two supertransition test temperatures, +75°F

and -200°F, and at one subtransition temperature, -321°F.

The fracture stress curve for tensile prestrain at test temperatures of +75°F and -200°F and the fracture stress curve for torsional prestrain at a test temperature of +75°F are all linear in nature with increasing magnitudes of prestrain.

But at a test temperature of -200°F, increasing torsional prestrain causes the fracture stress curve to remain horizontal for an interval of prestrain, and then the fracture stress rapidly decreases with further torsional prestrain. The shape of this curve is similar to that obtained for the SAE 1340 steel at a test temperature of -200°F for retained tensile ductility versus torsional prestrain, see Fig. 19.

For a test temperature of -321°F, the shape of the fracture stress versus tensile prestrain curve resembles that for the fracture stress versus torsional prestrain curve, in that with increasing prestrain each decreases to a minimum, then rises to a maximum value of fracture stress and then continues to decrease. These curves are somewhat similar in shape to those obtained for retained tensile ductility (-321°F) versus corresponding pre- strain, shown in Fig. 19 for SAE 1340 steel, i.e., for tensile prestrain the minima and maxima in the retained ductility curve, Fig. 19, and in the fracture stress curve, Fig. 25, occur at the same magnitude of tensile pre- strain. The same observations concerning the maxima and minima can be made with respect to torsional prestrain for the curves for retained ductility, Fig. 19, and for fracture stress, Fig. 25.

CONCLUSIONS

A correlation of the effects of tensile and torsional prestrain upon the tensile fracture properties for several metals at various test temperatures has indicated that for:

A. Copper

1. The curves for retained tensile ductility (+75°F and -321°F) versus prestrain were quite dissimilar in shape when the prestrain stress state was changed from torsion to tension.

2. The terminal points of the curves on the prestrain and retained ductility axes may be matched (after extrapolation of the supercritical branch of the torsional curve to the prestrain axis) by considering the torsional and tensile prestrain in terms of effective or generalized prestrain.

3. Tensile test specimens torsionally prestrained equivalent amounts exhibited similar fracture appearances at different test temperatures, whether the fracture was of the cup-cone or helical "wolf-ear" type. The "wolf-ear" tensile fracture was obtained after a critical magnitude of torsional prestrain which was the same for both test temperatures.

4. The attainment of the helical tensile fracture subsequent to critical or supercritical magnitudes of torsional prestrain was, in general, accompanied by a severe decrease in retained tensile ductility and fracture stress.

B. SAE 1020 Steel

1. For decreasing supertransition test temperatures, there was an increased degeneracy in the appearance of the helical "wolf-ear" tensile fracture subsequent to critical or supercritical magnitudes of torsional prestrain.

2. At subtransition test temperatures the "wolf-ear" type of tensile fracture essentially disappeared, being manifested only in helical surface markings on the broken tensile test specimen.

3. The degree of manifestation and the appearance of the helical "wolf-ear" fracture itself were dependent upon the tensile ductility for zero prestrain at the given test temperature.

4. The type of tensile fracture appearance obtained at any test temperature subsequent to a critical or upercritical magnitude of torsional prestrain was an effective compromise between two factors: (a) the propensity towards the helical type fracture and (b) the tensile fracture normally obtained for the non-prestrained metal at the given test temperature.

5. The critical magnitude of torsional prestrain necessary to attain the helical type of tensile fracture was relatively independent of test temperature.

6. Although there was rheotropic behavior in tension evidenced for both tensile and torsional prestrain, the stable branches of the retained tensile ductility curves for each type of prestrain did not extrapolate to the

same value of retained tensile ductility.

7. When effective prestrain was considered, the retained tensile ductility curves for the two types of prestrain matched only at the terminal points for a given test temperature.

8. Variation in prestrain stress state generally caused considerable variation in the shape of the curves for tensile fracture stress versus prestrain.

C. SAE 1340 Steel

1. No evidence of helical type tensile fracture was obtained.

2. Significant differences were obtained in the shape of the curves for retained tensile ductility versus prestrain and for tensile fracture stress versus prestrain by changing the prestrain stress state from tension to torsion.

3. Evidence of rheotropic behavior was obtained for both tensile and torsional prestrain at a subtransition test temperature ($-321^{\circ}F$).

ACKNOWLEDGMENTS

BIBLIOGRAPHY

(1) M. Gensamer, E. Saibel, J. T. Ransom and R. E. Lowne, The
Fracture of Metals, Am. Weld. Soc., New York (1947).

(2) G. Sachs, Effect of Strain on Fracture, in, Seminar on the
Fracturing of Metals, Am. Soc. Metals, Cleveland (1948).

(3) E. J. Ripling and W. M. Baldwin, Jr., Rheotropic Embrittle-
ment of Steel, Trans. Am. Soc. Metals, Vol 43 (1951). pp. 778-810

(4) H. W. Swift, Tensional Effects of Torsional Overstrain in Mild
Steel, J. of Iron and Steel Inst., Vol. 140 (1939) pp. 181-211.

(5) W. A. Backofen, A. J. Shaler and B. B. Hundy, Mechanical Anisotropy
in Copper, Trans. Am. Soc. Metals, Vol. 46 (1954) pp. 655-680.

(6) W. A. Backofen and B. B. Hundy, Mechanical Anisotropy in Some
Ductile Metals, J. of Inst. of Metals., Vol. 81 (1952-53), pp. 433-438.

(7) S. I. Liu, The Flow and Fracturing Characteristics of the Aluminum
Alloy 24S-T4 as Affected by Strain-Thermal History, Case Inst. of
Technology, ONR Tech. Report No. 19, Contract No. N6-ori-273/I,
(Nov. 1949).

(8) E. J. Ripling and W. M. Baldwin, Jr., Overcoming Rheotropic Brittle-
ness: Precompression Versus Pretension, Trans. Am. Soc. Metals,
Vol. 44 (1952) pp. 1047-1057.

(9) E. A. Saibel, Final Report on the Extension of the Thermodynamic
Theory of the Strength of Metals, Contract No. 6S-34023, Job Order
No. 1, (July 1946).

(10) R. E. Peterson, Stress Concentration Design Factors, John Wiley
and Sons, Inc. (1953) p. 67.

(11) A. A. Griffith, Theory of Rupture, Proceedings, First International
Congress for Applied Mechanics, Vol. 55, Delft (1924).

(12) M. Gensamer, Strength of Metals Under Combined Stresses, Am.
Soc. Metals (1940).

(13) C. Zener and J. H. Hollomon, Plastic Flow and Rupture of Metals,
Trans. Am. Soc. Metals, Vol. 33 (1944) pp. 163-235.

(14) A. Nadai, Plasticity, McGraw-Hill (1931).

(15) L. R. Jackson, Work Hardening and Rupture in Metals, Metals
Technology, Vol. 13 (Oct. 1946).

(16) W. T. Lankford, J. R. Low and M. Gensamer, The Plastic Flow
of Aluminum Alloy Sheet Under Combined Loads, Metals Technology,
Vol. 14 (Aug. 1947).

(17) D. S. Fields, Jr., W. A. Backofen and J. Wulff, Mechanical Anisotropy
in SAE 4340 Steel, Massachusetts Inst. of Technology, ONR Tech.
Report No. 4, Contract No. N5ori-07841 (Sept. 1953).

(18) A. S. Eldin and S. C. Collins, Fracture and Yield Stress of 1020 Steel
at Low Temperature, J. of Applied Physics, Vol. 22 (Oct. 1951)
pp. 1296-1297.

(19) E. J. Ripling and G. Tuer, An Apparatus for Tensile Testing at Sub-
Zero Temperatures, Product Engineering, Vol. 20, No. 1 (1949)
pp. 103-105.

APPENDIX

Details of Material and Procedure

Material

All material used in this investigation was received in the form of 3/4 inch diameter hot rolled rods. The chemical analyses of the copper and the two steels used are shown in Table I.

Table I - Chemical Analyses

Material	Per Cent						
	C	Si	Mn	P	S	Cu	Fe
Copper					.003	99.95	.02
SAE 1020 steel	.199	.10	.73	.009	.044		
SAE 1340 steel	.364	.30	1.68	.013	.028		

All of the rods of SAE 1020 steel used in this investigation were rolled from a single billet of aluminum-killed steel. Also, all of the SAE 1340 steel rods used in this investigation were rolled from one billet.

Heat Treatment

Copper - The copper rods were annealed at 900°F for one hour and then air cooled.

SAE 1020 Steel - Rods of this material were annealed at 1700°F for 1-3/4 hours, furnace cooled to room temperature, spheroidized at 1300°F for 120 hours and finally furnace cooled.

SAE 1340 Steel - Rods of this material were normalized at 1675°F for 1/2 hour and then air cooled. These normalized rods were next stress-relieved at 1200°F for 4 hours and were then furnace cooled.

Torsional prestrain specimens of the type shown in Fig. 3b were rough-machined from the normalized and stress-relieved material, leaving sufficient grinding stock on the specimens. Next the oversize specimens were austenitized at 1525°F for 3/4 hour, water quenched, tempered at the required temperature for one hour and finish ground.

The preparation of the tensile prestrain specimens varied somewhat from that given above. After normalizing and stress-relieving the rods according to the above schedule, they were rough-machined into 0.55 inch cylinders, water quenched and tempered according to the above schedule, and finally finish-ground to the dimensions shown in Fig. 3a. The modification in the procedure (rough machining 0.55 inch cylinders) was necessary to ensure good agreement in mechanical properties and microstructure between a tensile test specimen (Fig. 3a) heat treated and machined according to this procedure and a tensile test specimen (Fig. 3a) machined from the reduced section (Fig. 3b) of a non-prestrained torsional prestrain specimen.

Microstructures after heat treatment for all materials used in this investigation are shown in Fig. 26.

Specimens

The torsional prestrain specimens for all the materials used in this investigation were of the type shown in Fig. 3b. The reduced section only of the specimen was actually twisted, the ends of the specimen being restrained in the jaws of the torsion machine.

Tensile test specimens of the type shown in Fig. 3a were machined from the center of the reduced section of the prestrained torsion specimen.

All of the torsionally prestrained copper specimens were finished to a tensile test specimen of a diameter of 0.212 inch at the minimum section, as were all tensile test specimens of the spheroidized SAE 1020 steel tested at temperatures above -280°F.

At test temperatures below -280°F, tensile test specimens of the spheroidized SAE 1020 steel had to be finish-machined to a diameter of 0.180 inch at the minimum section in order to avoid specimen shoulder fractures and to prevent damage to the tensile testing equipment. Also, for the above reasons, all tensile test specimens made from the quenched and tempered SAE 1340 steel were finished to a diameter of 0.180 inch.

Equipment and Test Procedure

A commercial type torsion machine with a 10,000 pound-inch maximum torque capacity was used to effect torsional prestrain. All torsional pre-strains were performed at a strain rate of 120 degrees per minute.

A 60,000 pound capacity commercial type hydraulic tensile testing machine was used for both tensile prestrain and for the subsequent tensile test after either torsional or tensile prestrain. A specially constructed loading fixture (19) yielding an excentricity of less than 0.001 inch was used for both the tensile prestraining and tensile testing.

The time interval between the tensile prestrain and the tensile test was about four hours; but when the prestrain was torsional in nature, the

interval between prestrain and tensile test was longer (72 hours) because of the time required to machine a tensile test specimen from a specimen prestrained in torsion.

The magnitudes of tensile prestrain and of retained tensile ductility were obtained by means of diameter measurements made with a micro-comparator prior to and subsequent to each particular strain.

The coolants used for the low temperature tests were:

-40°F to -110°F	Isopentane and dry ice
-110°F to -240°F	Isopentane and liquid nitrogen
-260°F to -300°F	Nitrogen vapor from boiling liquid nitrogen
-321°F	Liquid nitrogen at boiling point
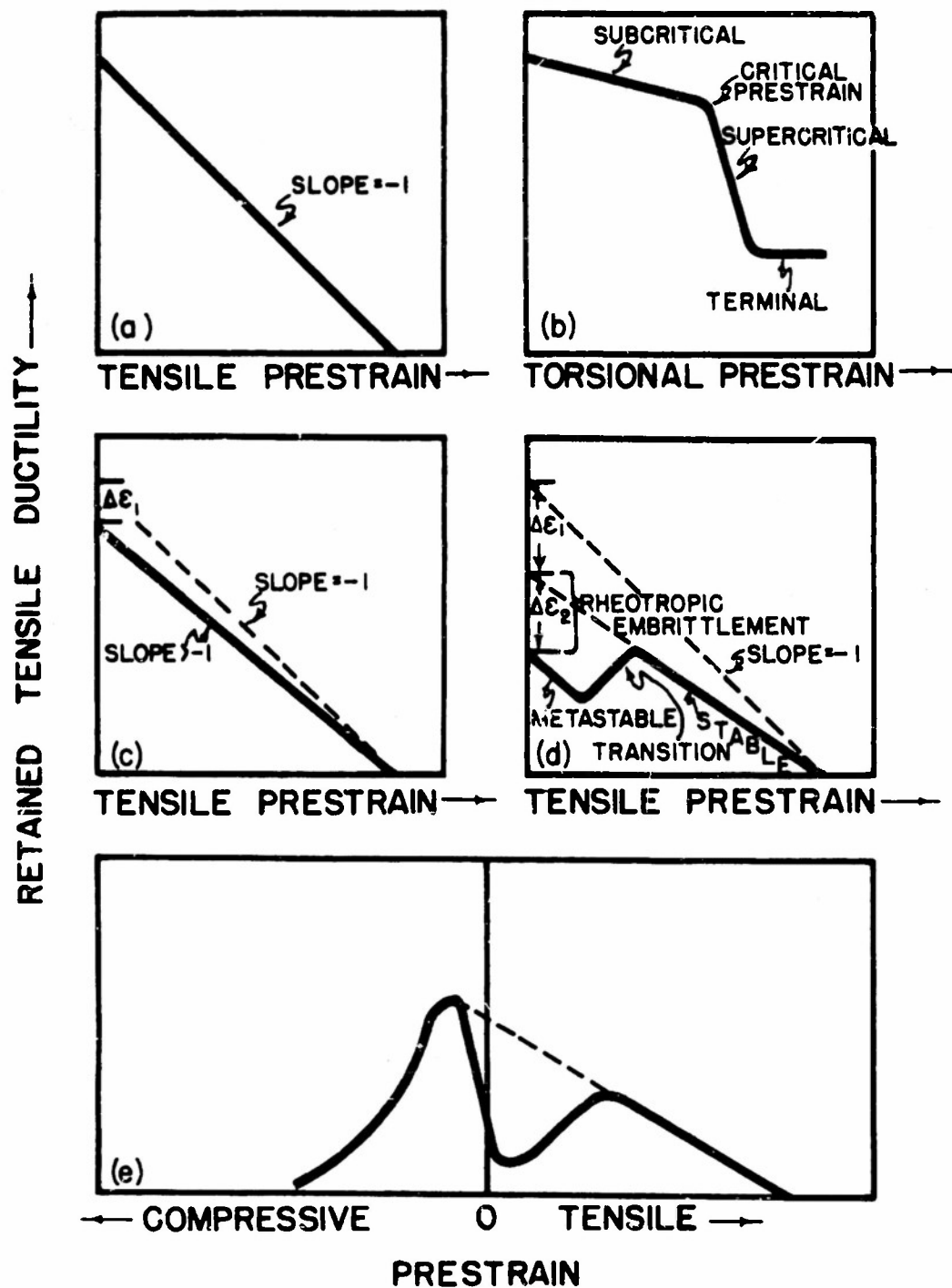
FIG. 1 : SCHEMATIC DRAWINGS OF THE RELATIONSHIPS BETWEEN RETAINED TENSILE DUCTILITY AND PRESTRAIN (TENSILE, TORSIONAL OR COMPRESSIVE).
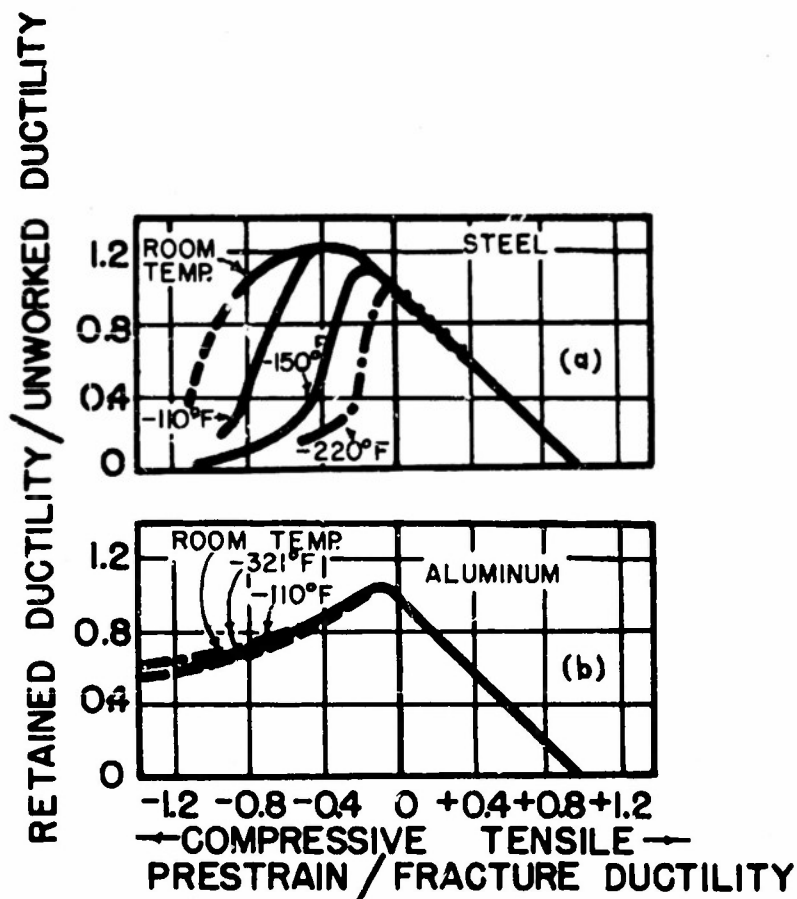
FIG. 2 : EFFECT OF TEST TEMPERATURE ON TENSILE
DUCTILITY SUBSEQUENT TO PRESTRAIN. (SAE 1340
STEEL DATA FROM RIPLING AND BALDWIN (8);
24S-T4 ALUMINUM DATA FROM LIU(7).
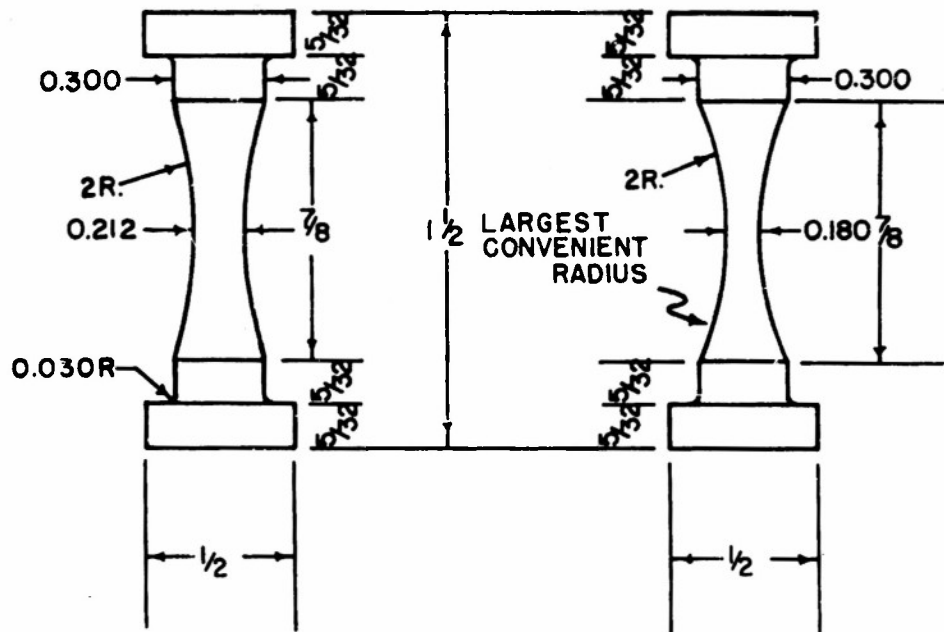
(a) TENSILE PRESTRAIN OR TEST SPECIMENS.
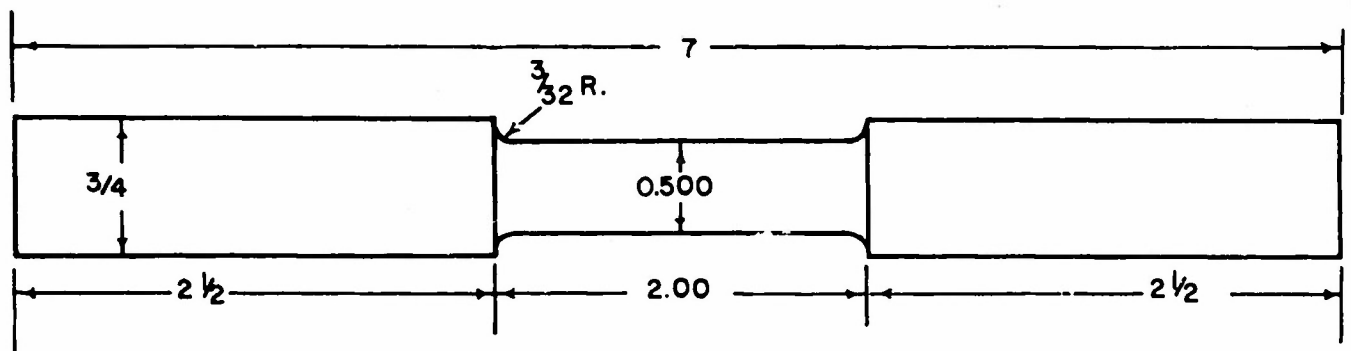
(b) TORSIONAL PRESTRAIN SPECIMEN.

FIG. 3 : PRESTRAIN AND TENSILE TEST SPECIMENS.
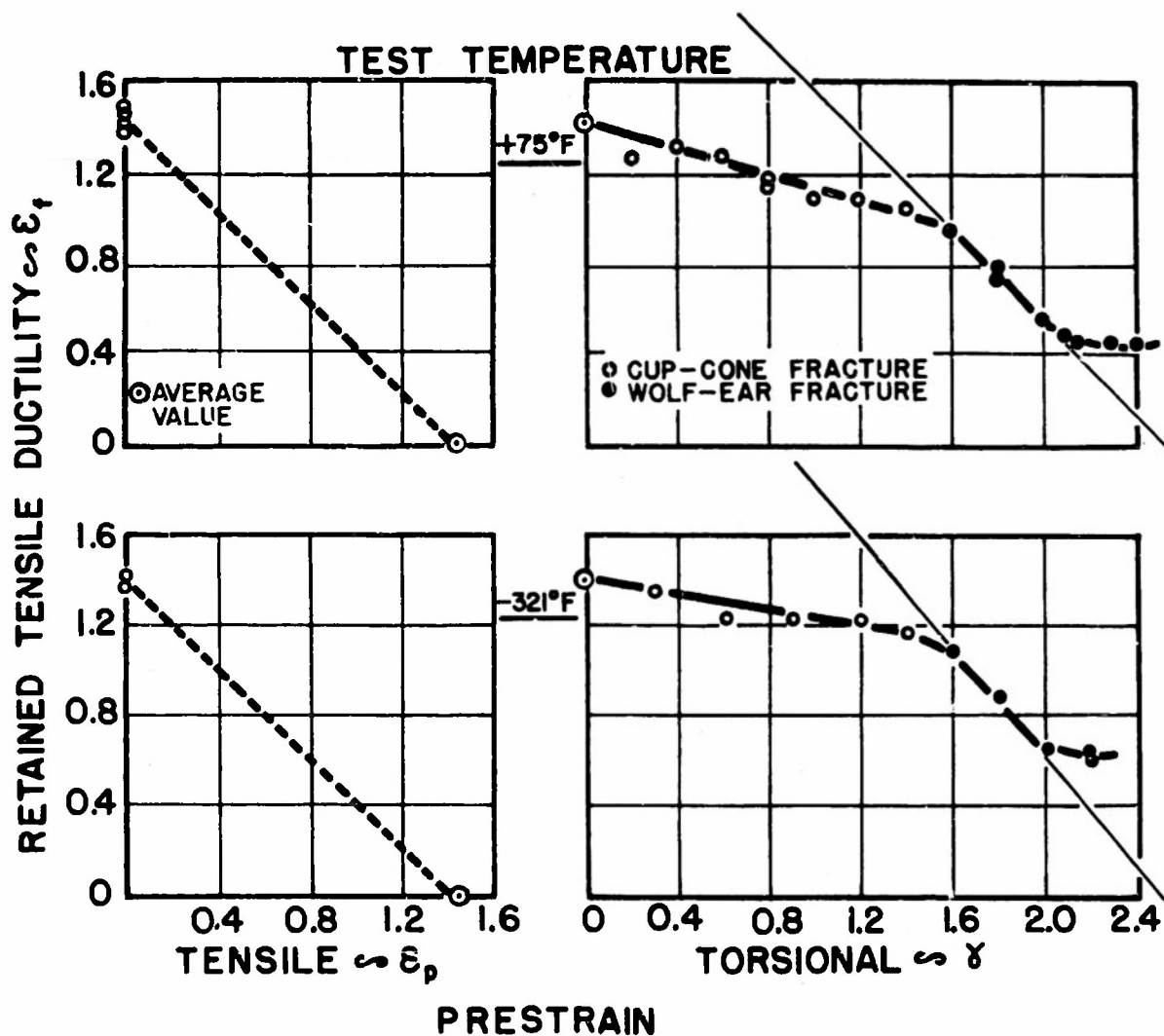
FIG. 4 : EFFECT OF TEST TEMPERATURE UPON THE RETAINED
TENSILE DUCTILITY OF ANNEALED ELECTROLYTIC
TOUGH PITCH COPPER SUBSEQUENT TO TENSILE
OR TORSIONAL PRESTRAIN (+75°F).

$\gamma =$ 0.00   1.60   2.00   2.20

$+ 75°F$

$\gamma =$ 0.00   1.60   2.00   2.30

$- 321°F$
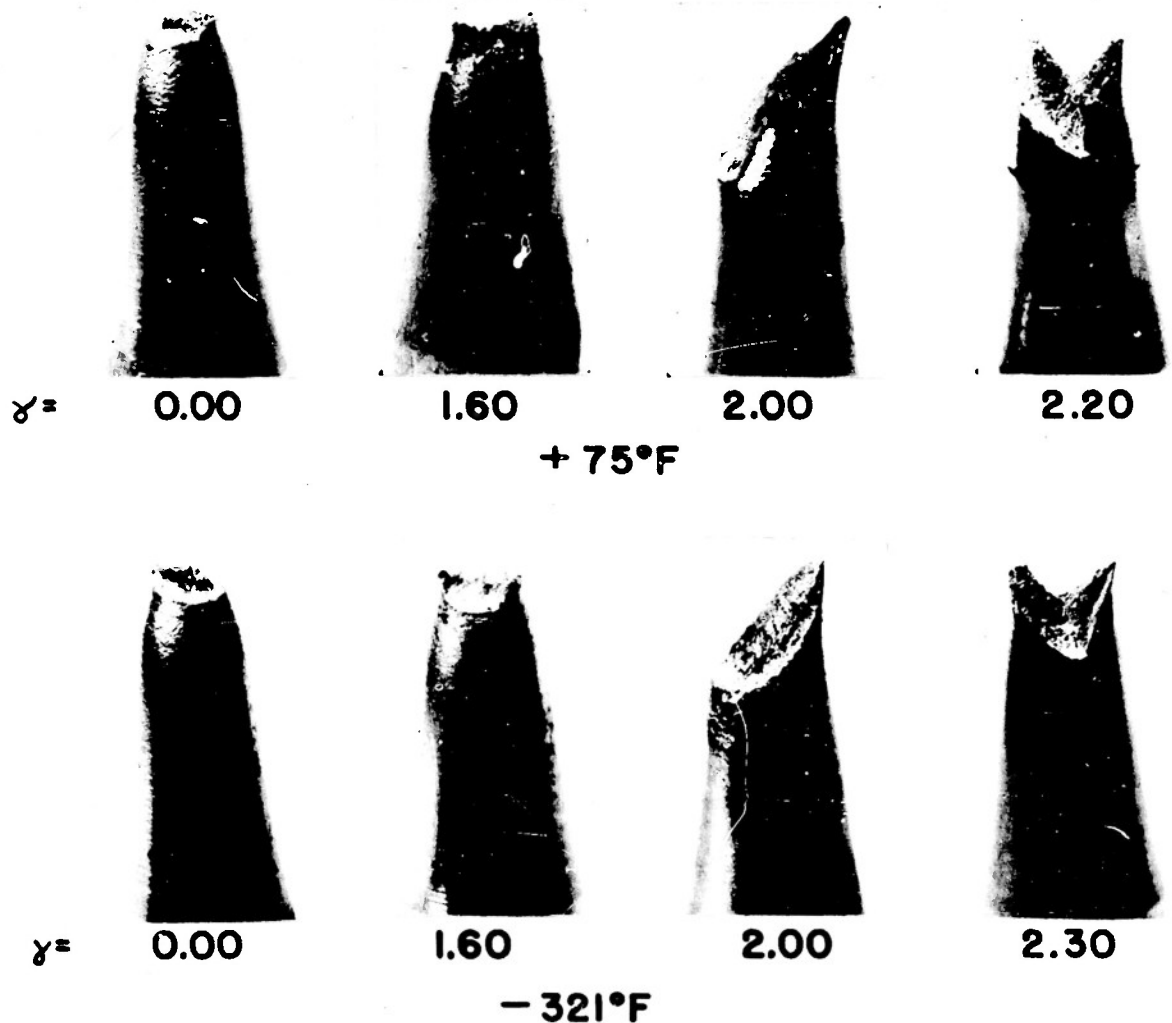
FIG. 5 : TENSILE FRACTURES FOR ELECTROLYTIC TOUGH PITCH COPPER PRESTRAINED TO INDICATED SURFACE SHEAR STRAIN (γ) AND TESTED AT INDICATED TEMPERATURE. MAGNIFICATION APPROXIMATELY 4X.
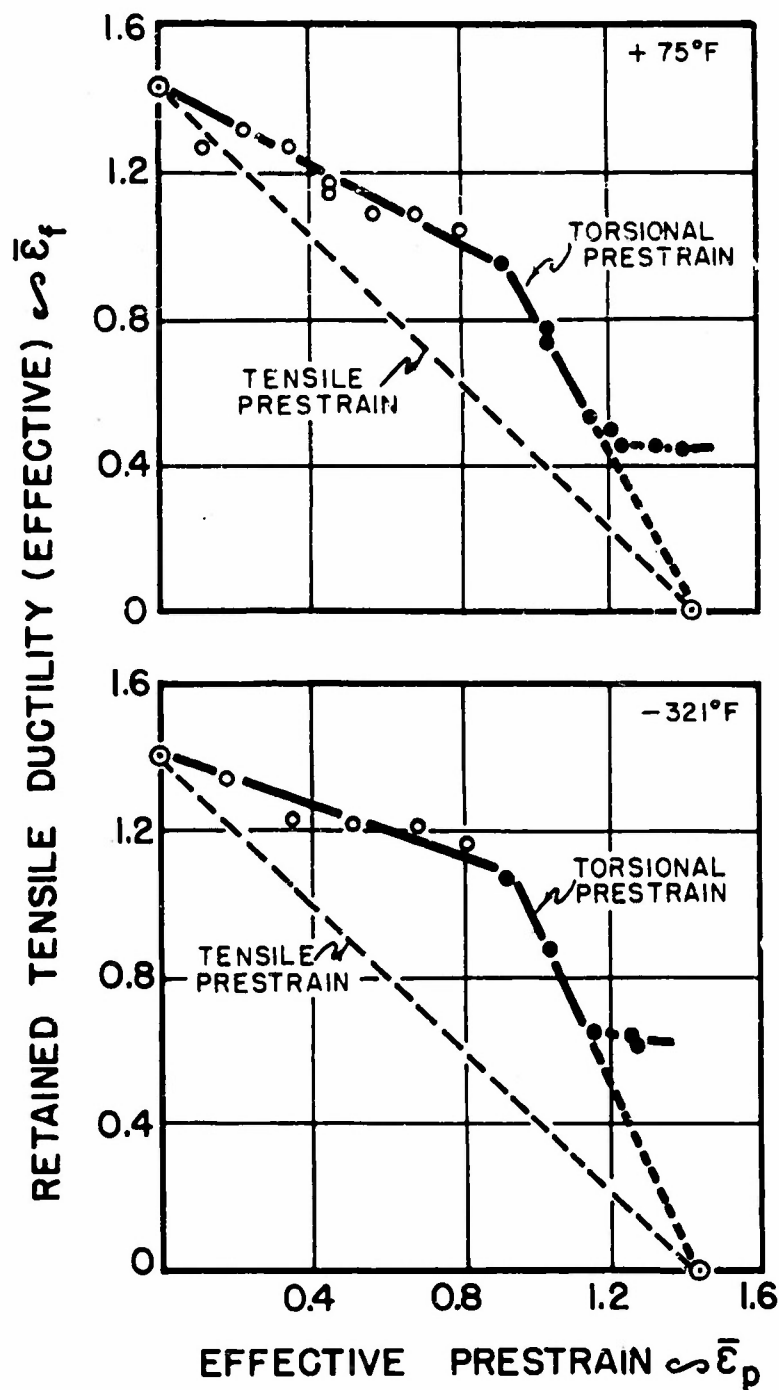
FIG.6: EFFECT OF TEST TEMPERATURE UPON THE RETAINED
TENSILE DUCTILITY OF ANNEALED ELECTROLYTIC
TOUGH PITCH COPPER SUBSEQUENT TO EFFECTIVE
PRESTRAIN (+75°F).
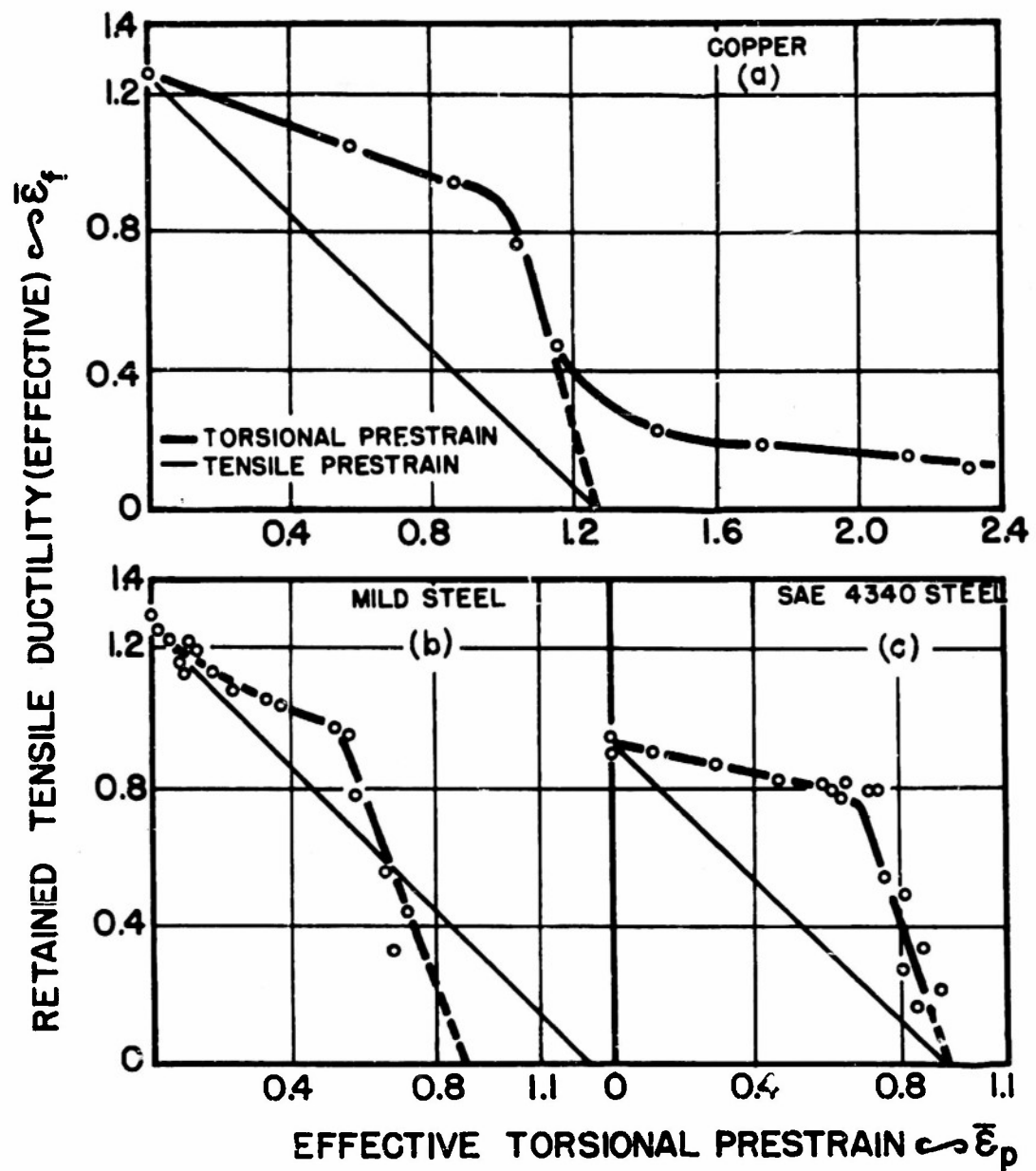
FIG. 7: EFFECT OF TORSIONAL PRESTRAIN UPON THE
RETAINED TENSILE DUCTILITY. (DATA FOR COPPER
BACKOFEN(5); DATA FOR MILD STEEL BY SWIFT(4);
DATA FOR SAE 4340 STEEL BY FIELDS (17))
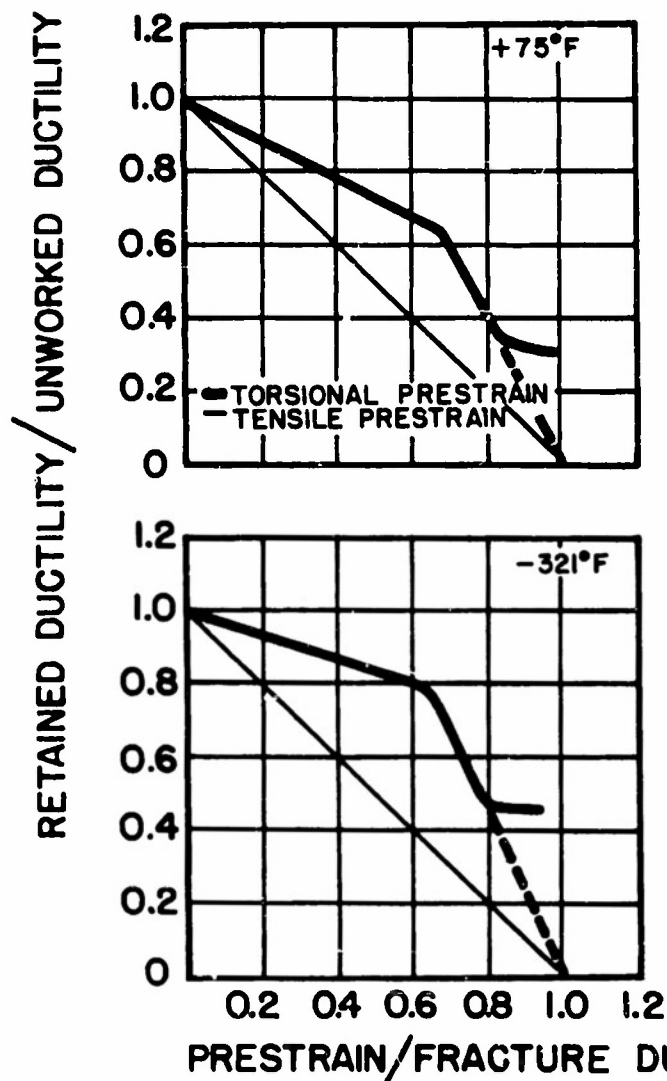
FIG. 8 : EFFECT OF TEST TEMPERATURE ON THE TENSILE
DUCTILITY OF ANNEALED ELECTROLYTIC TOUGH
PITCH COPPER SUBSEQUENT TO TENSILE OR
TORSIONAL PRESTRAIN.
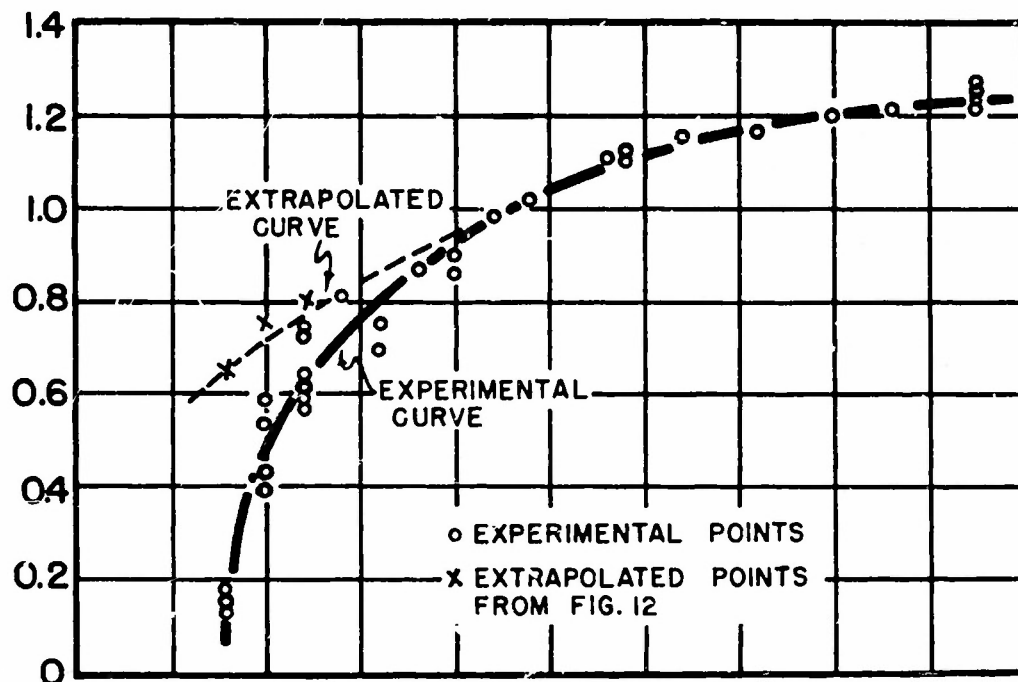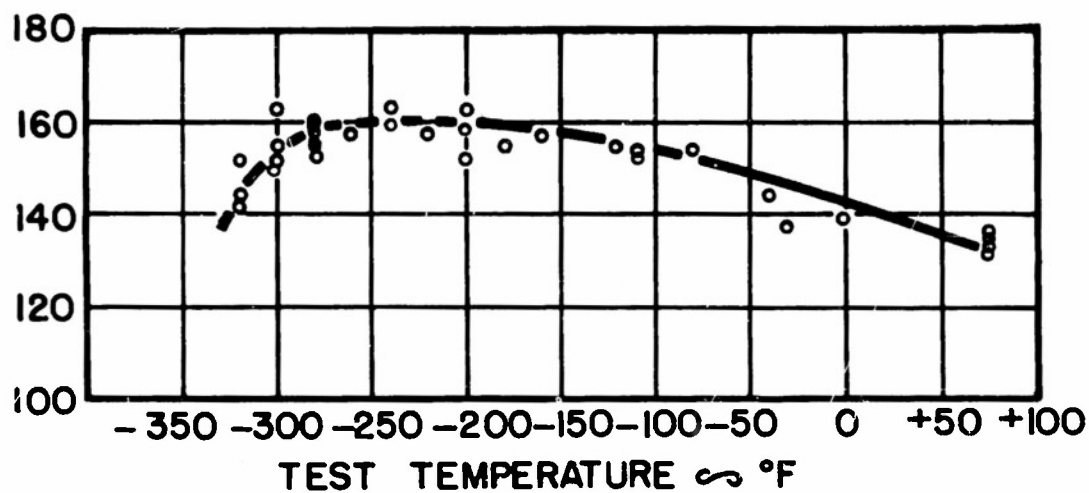
FIG. 9 : THE EFFECT OF TEST TEMPERATURE UPON THE
TENSILE FRACTURE PROPERTIES OF SPHEROIDIZED
SAE 1020 STEEL.
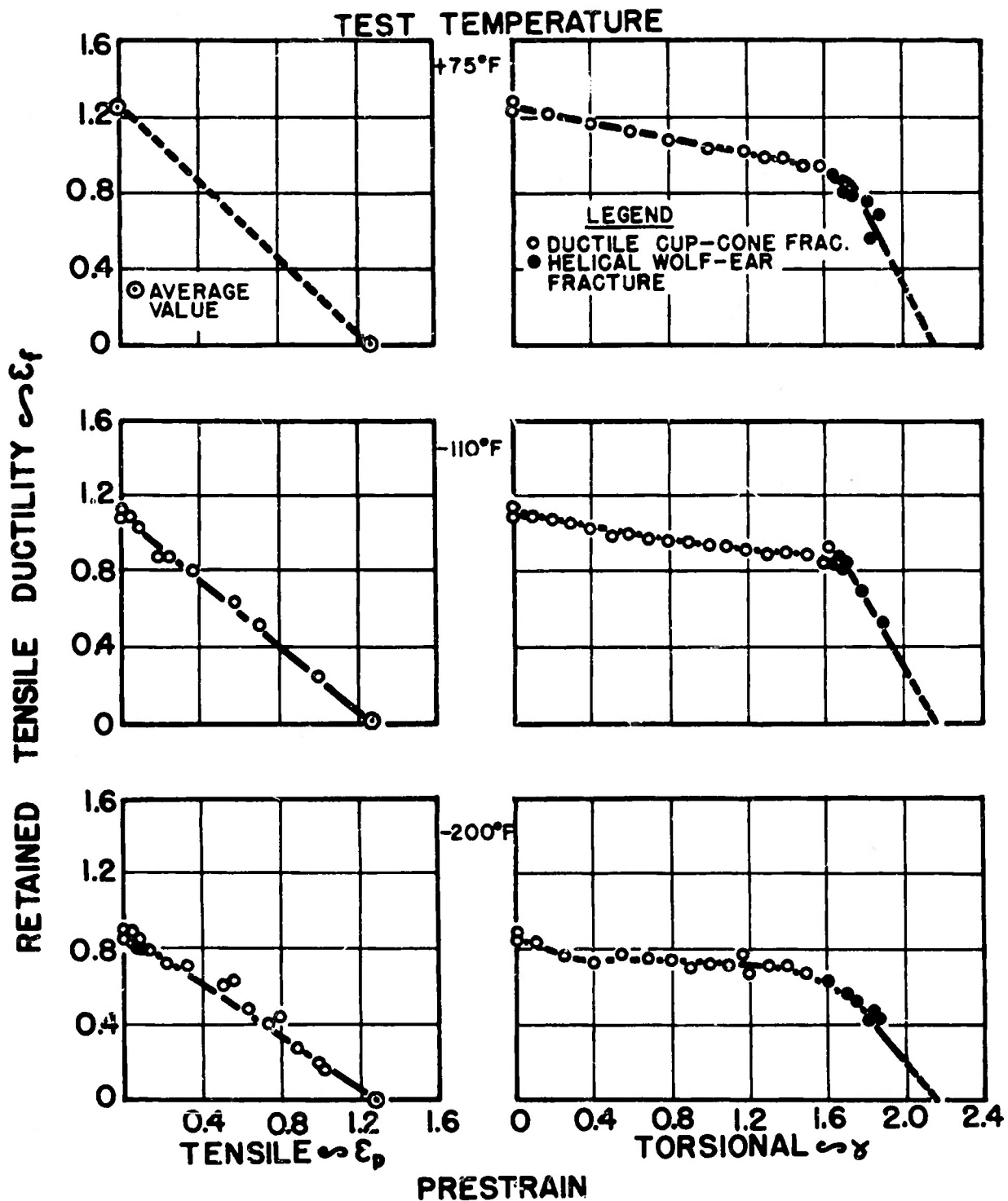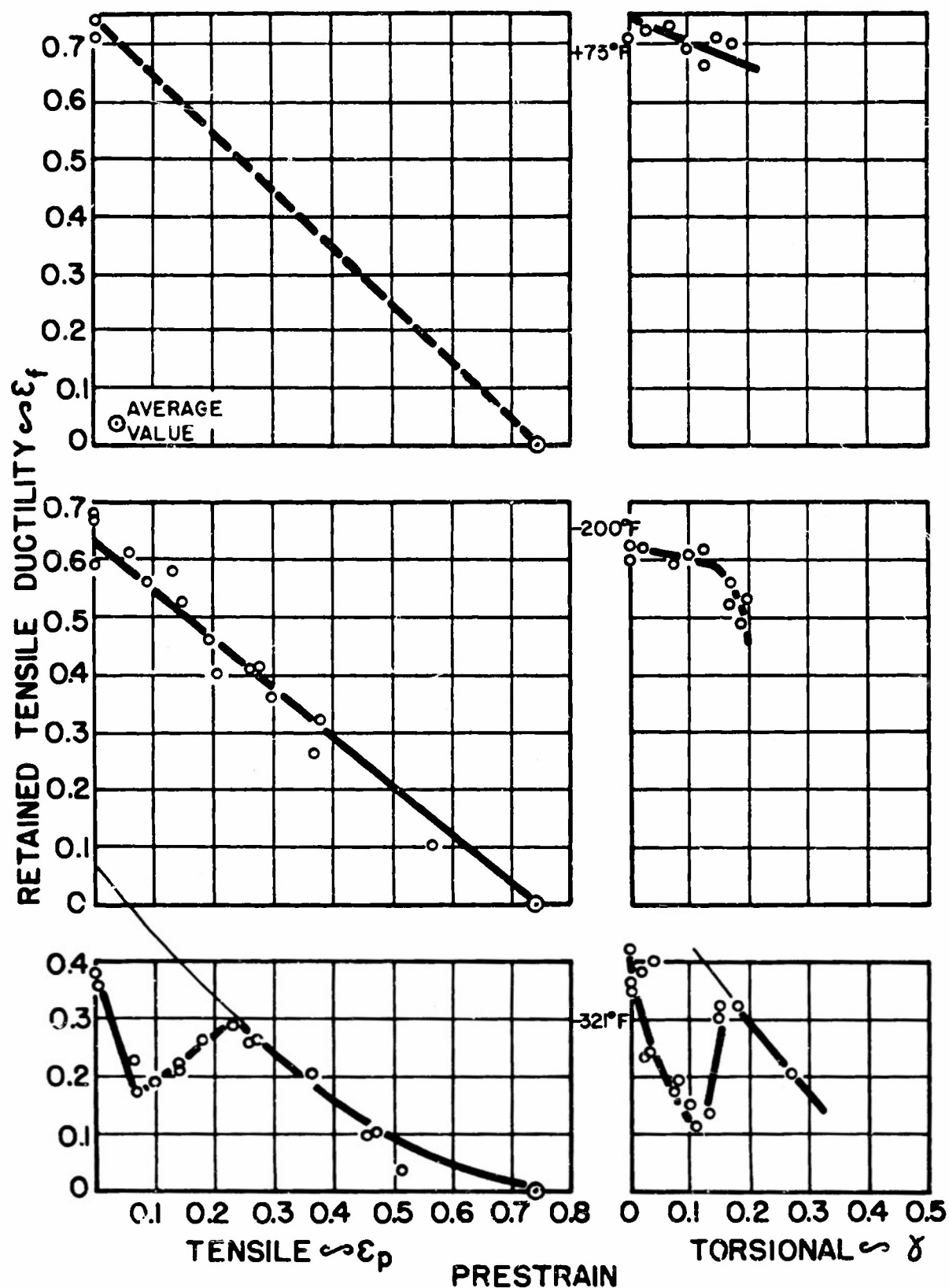
FIG. 10: EFFECT OF TEST TEMPERATURE UPON THE RETAINED
TENSILE DUCTILITY OF SPHEROIDIZED SAE 1020 STEEL
SUBSEQUENT TO TENSILE OR TORSIONAL PRESTRAIN
(+75°F).

A   B   C

$\gamma =$ 0.00   1.65   1.90

+75°F

$\gamma =$ 0.00   1.62   1.90

−110°F

$\gamma =$ 0.00   1.60   1.86

−200°F
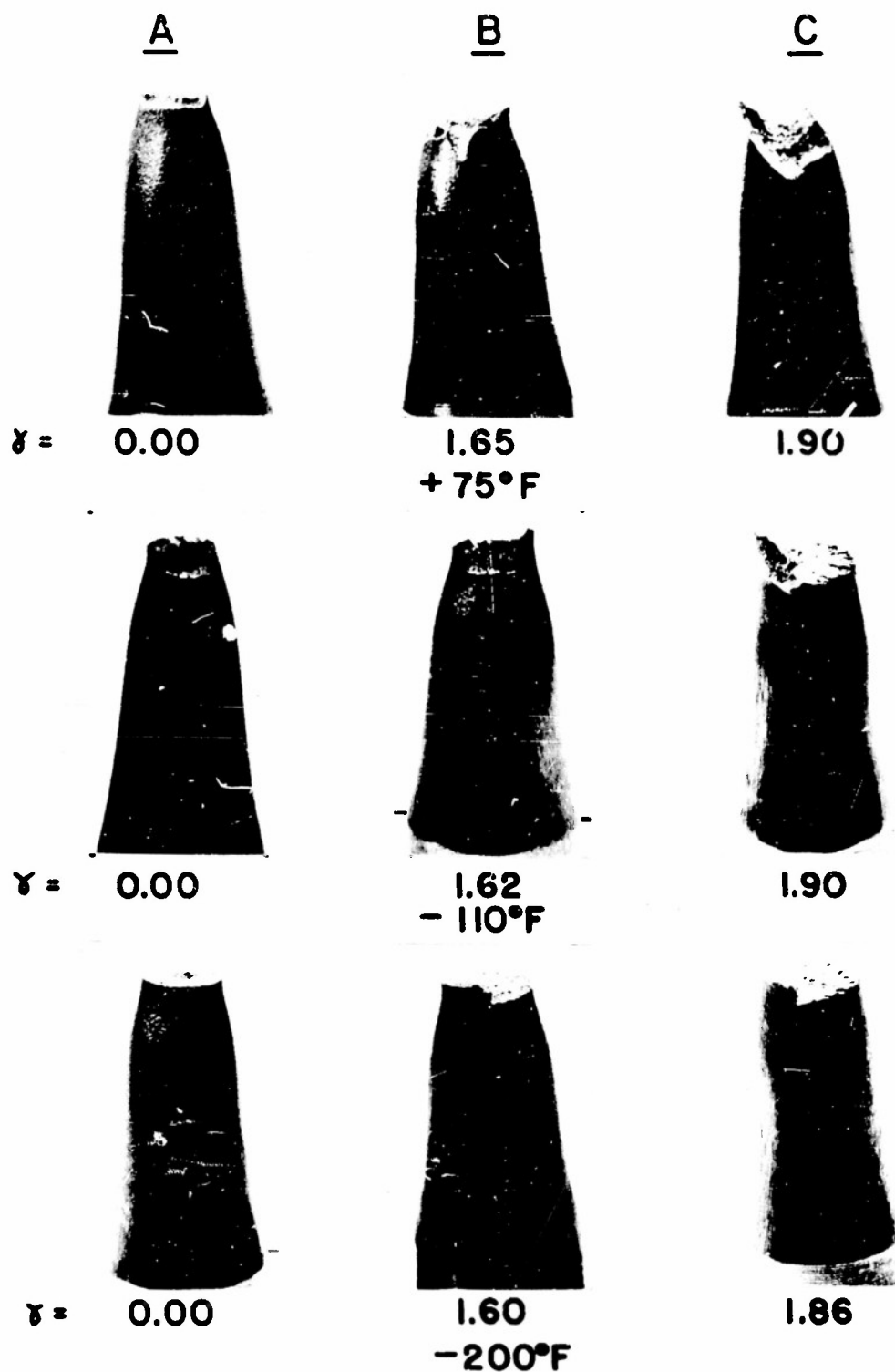
FIG. 11 : TENSILE FRACTURES FOR SPHEROIDIZED SAE 1020 STEEL PRESTRAINED TO INDICATED SURFACE SHEAR STRAIN (γ) AND TESTED AT INDICATED TEMPERATURE. MAGNIFICATION APPROXIMATELY 4X.
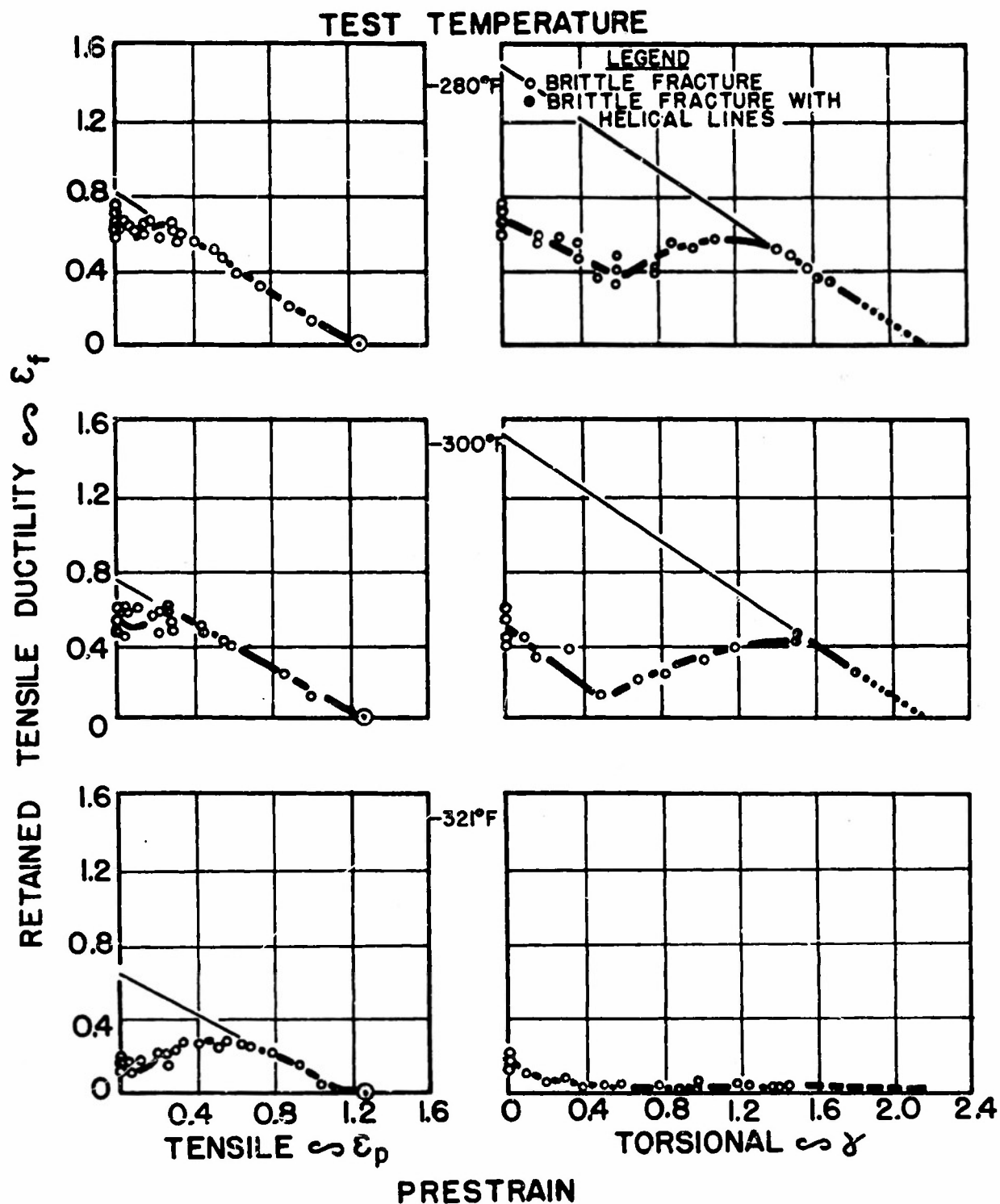
FIG.12 : EFFECT OF TEST TEMPERATURE ON THE RETAINED
TENSILE DUCTILITY OF SPHEROIDIZED SAE 1020 STEEL
SUBSEQUENT TO TENSILE OR TORSIONAL PRESTRAIN
(+75°F).
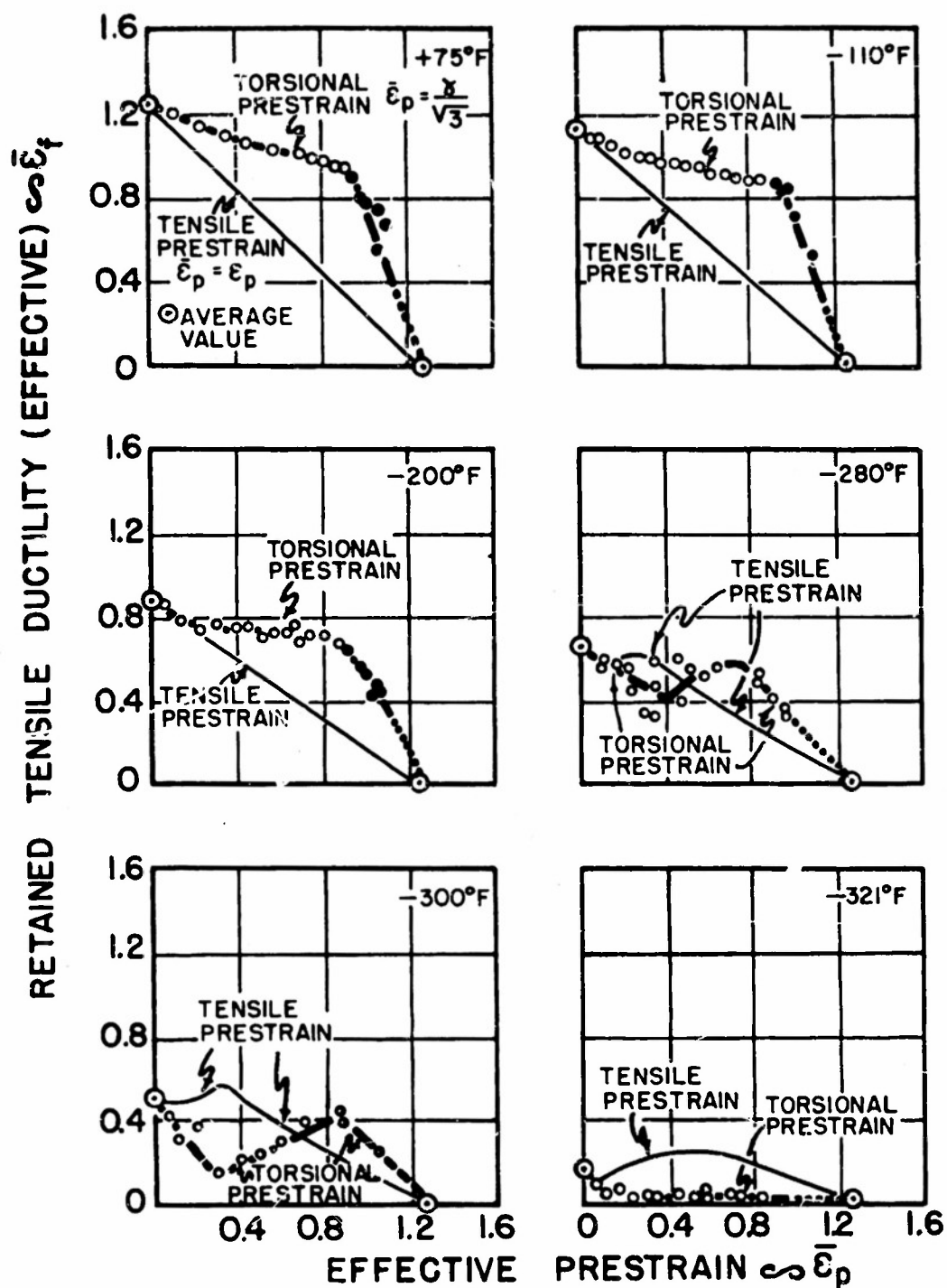
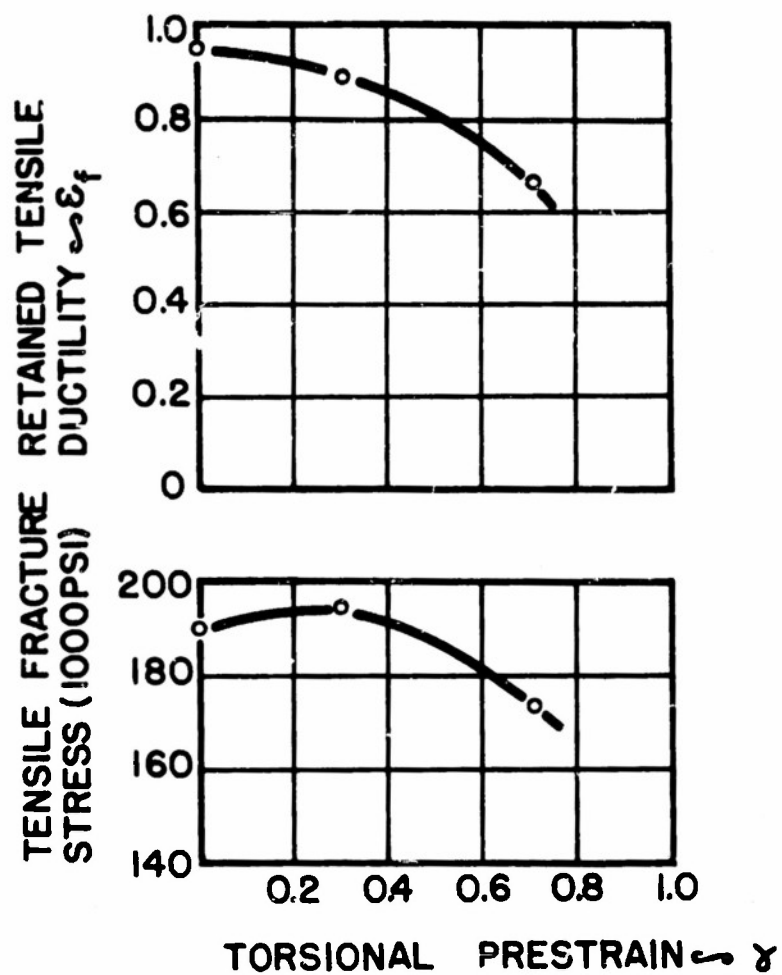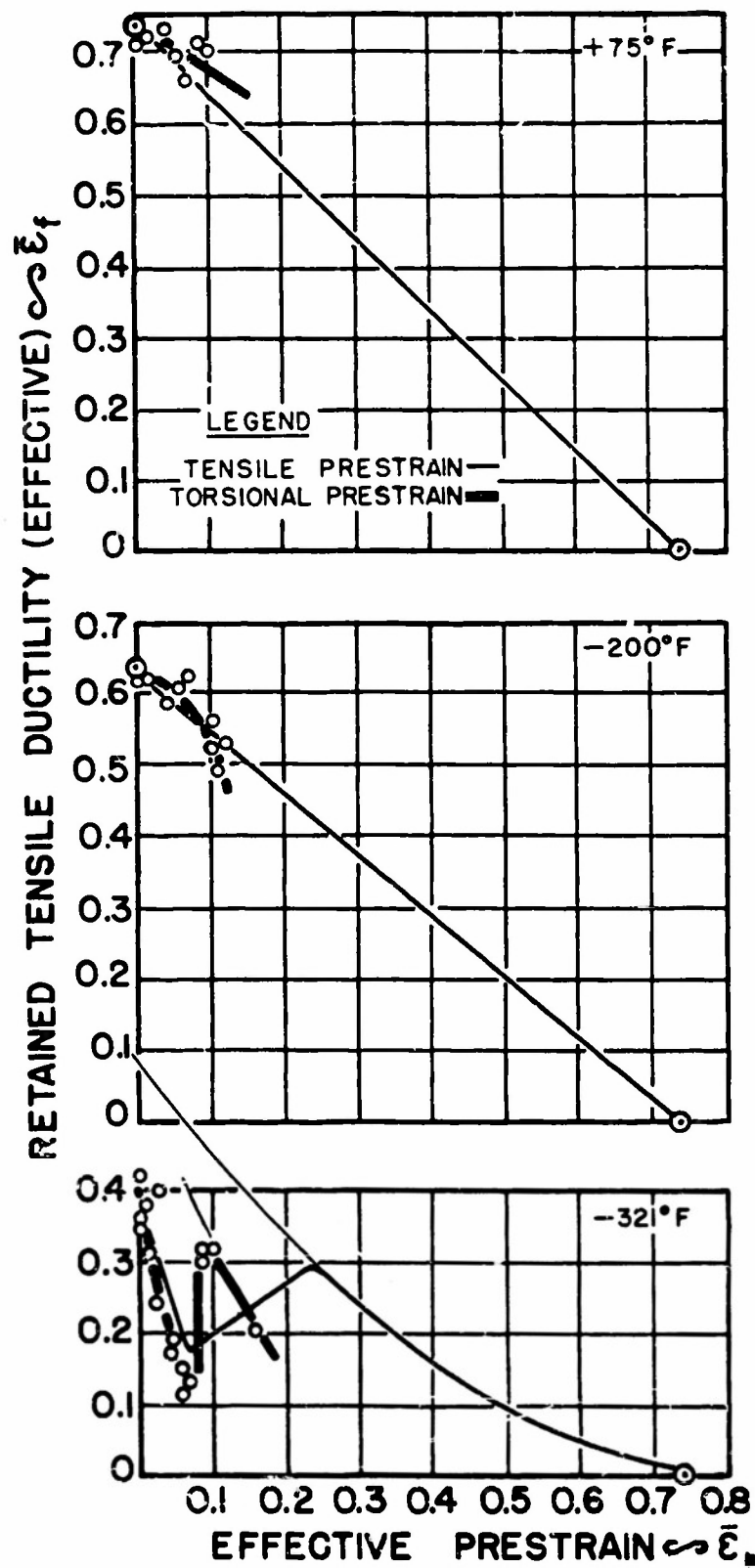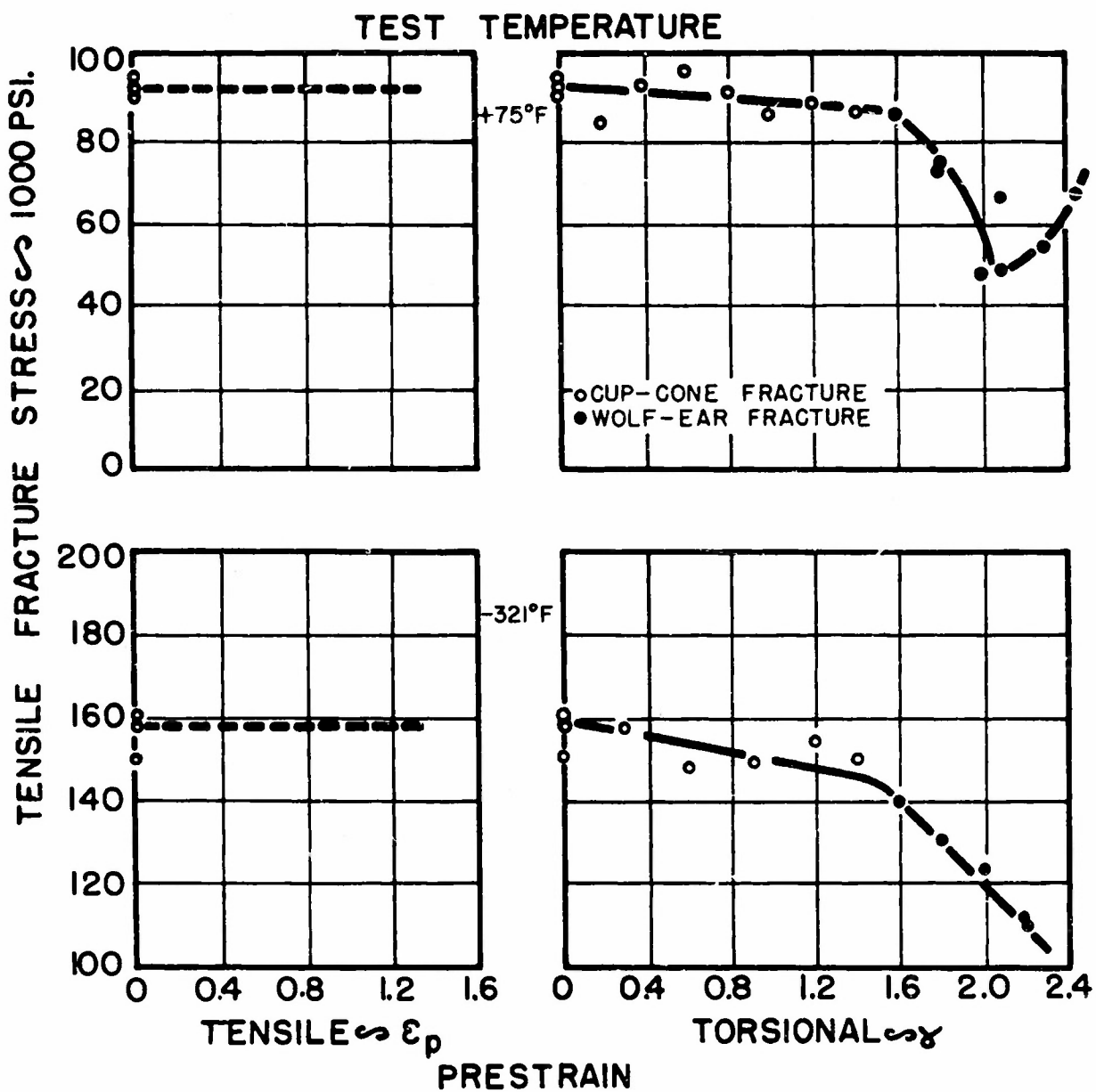FIG. 13 : EFFECT OF TEST TEMPERATURE ON THE RETAINED
TENSILE DUCTILITY OF SPHEROIDIZED SAE 1020 STEEL
SUBSEQUENT TO TENSILE OR TORSIONAL PRESTRAIN
(+ 75°F).
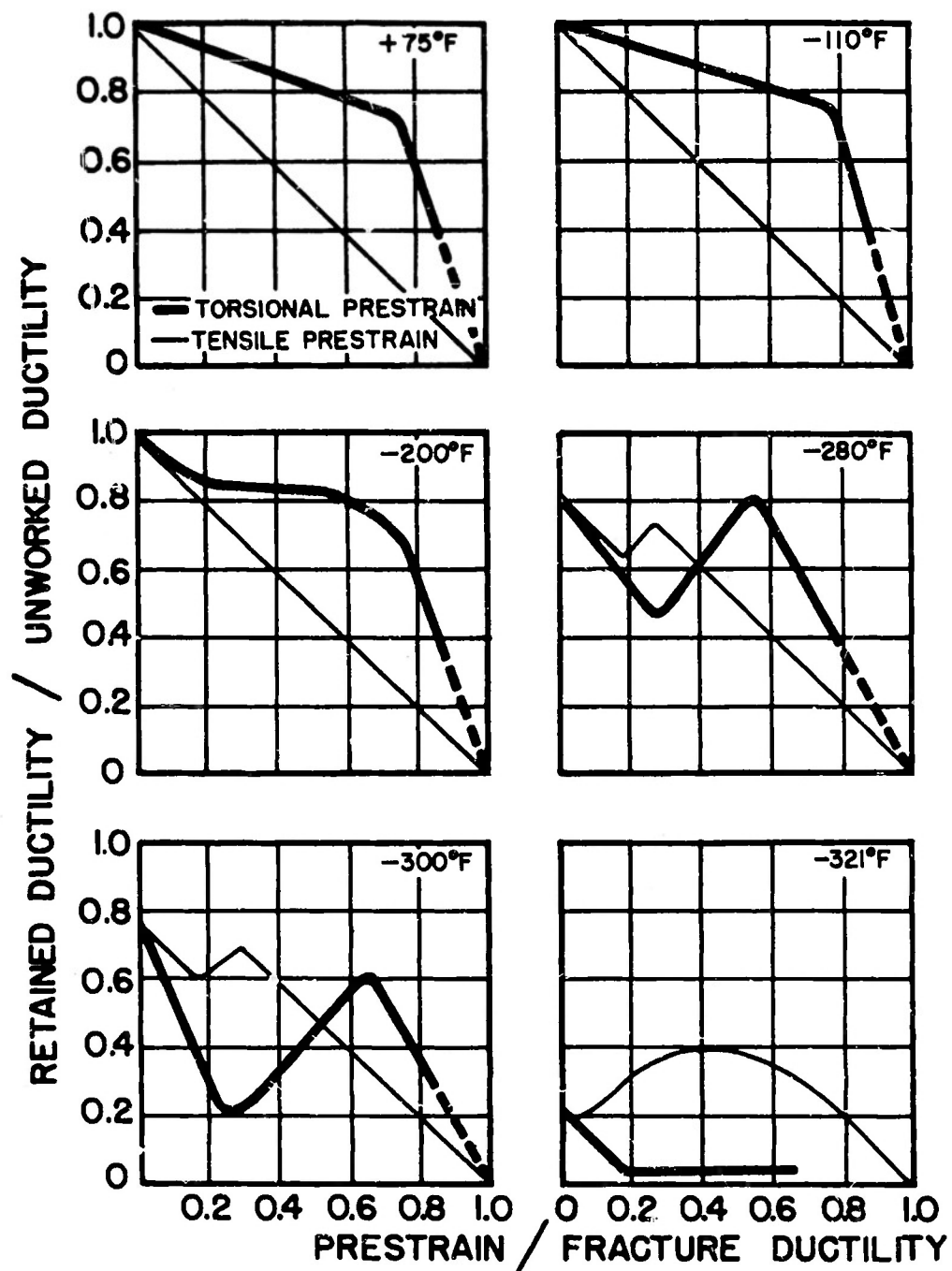
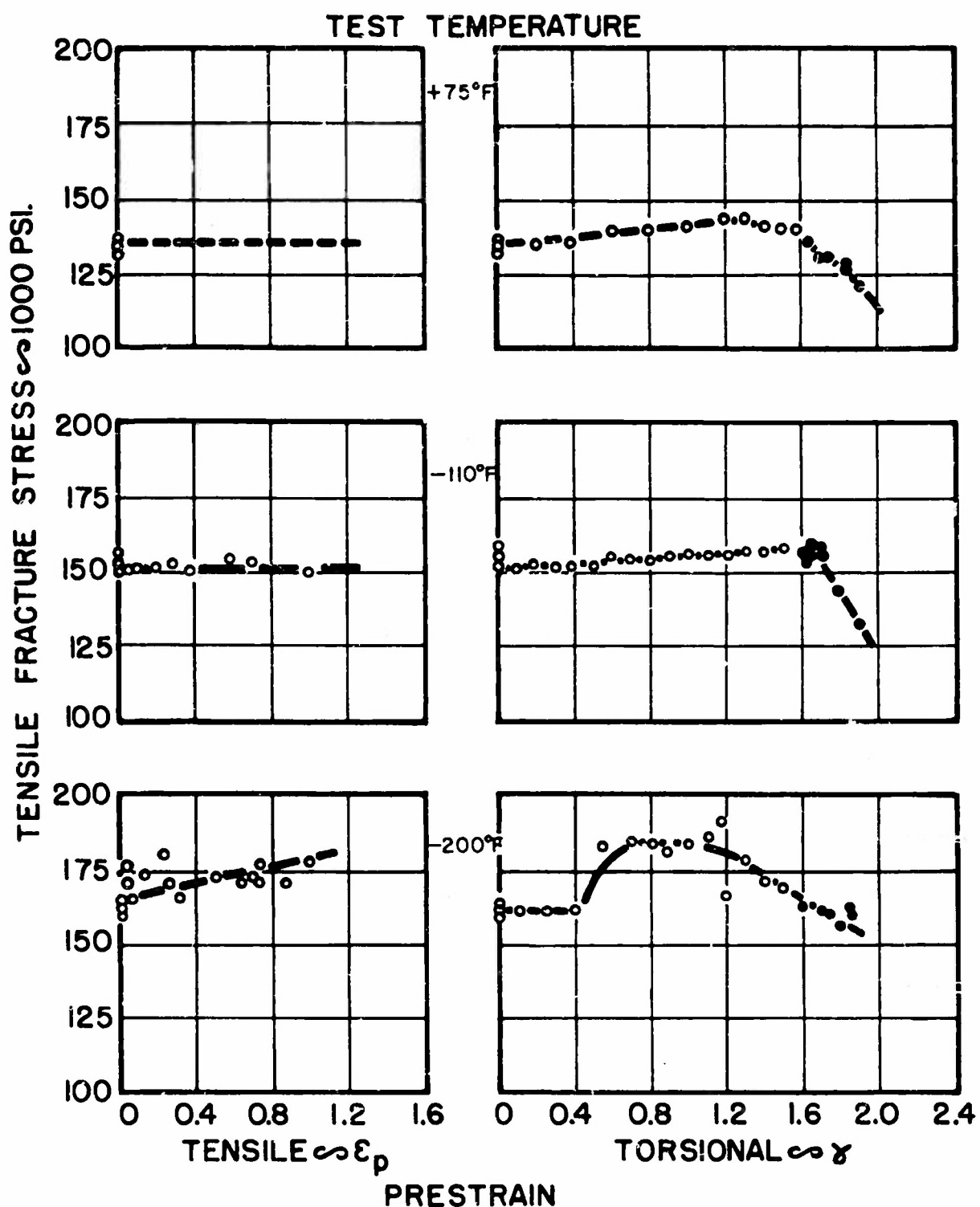FIG. 14 : EFFECT OF TEST TEMPERATURE ON THE TENSILE
DUCTILITY OF SPHEROIDIZED SAE 1020 STEEL
SUBSEQUENT TO TENSILE OR TORSIONAL PRESTRAIN.
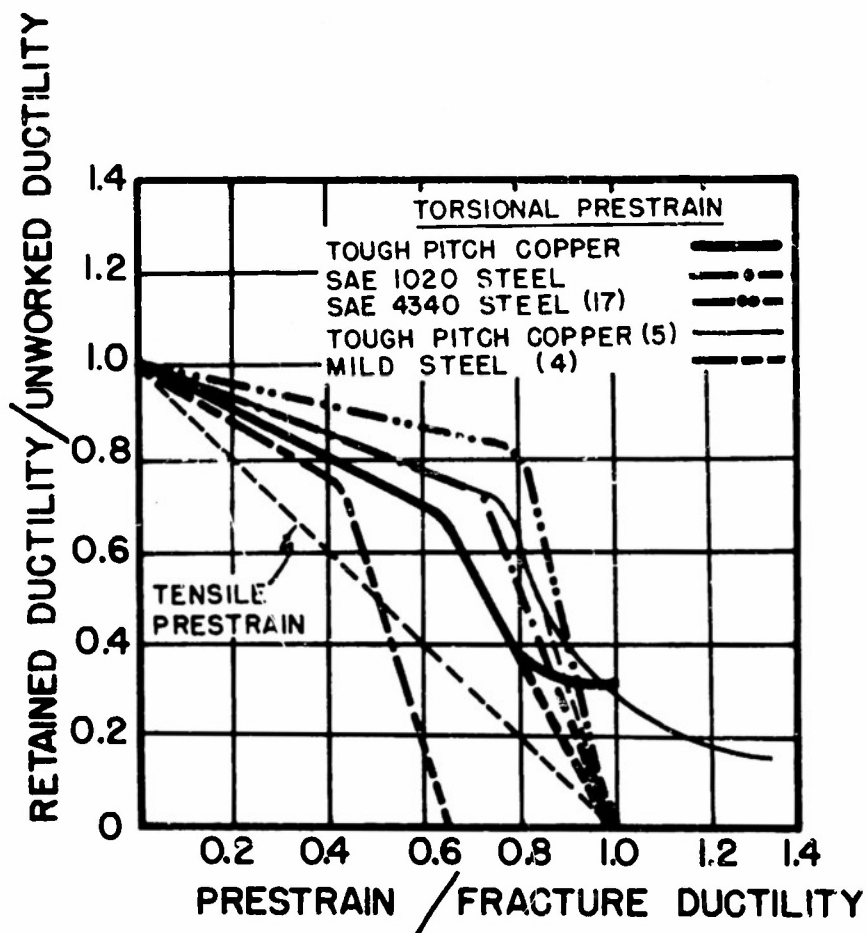
FIG.15: EFFECT OF TORSIONAL OR TENSILE PRESTRAIN AT ROOM TEMPERATURE UPON THE RETAINED TENSILE DUCTILITY AT ROOM TEMPERATURE. (DATA FOR MILD STEEL FROM SWIFT (4); DATA FOR TOUGH PITCH COPPER FROM BACKOFEN (5); AND DATA FOR 4340 STEEL FROM FIELDS (17)).
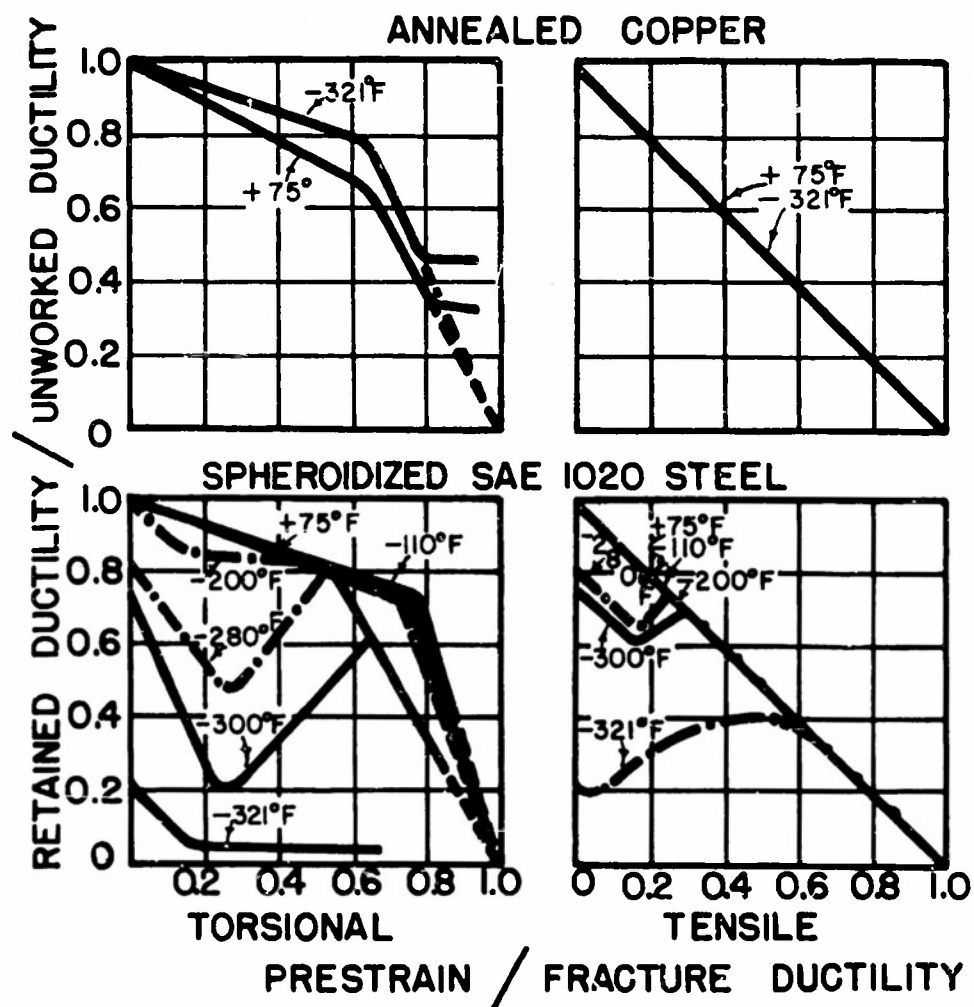
FIG. 16 : EFFECT OF TEST TEMPERATURE ON TENSILE DUCTILITY SUBSEQUENT TO TORSIONAL OR TENSILE PRESTRAIN.
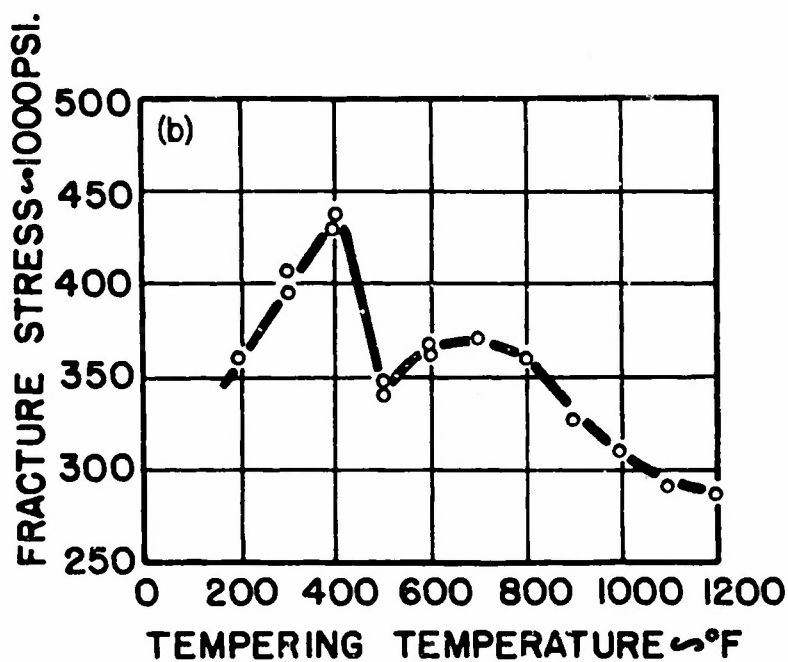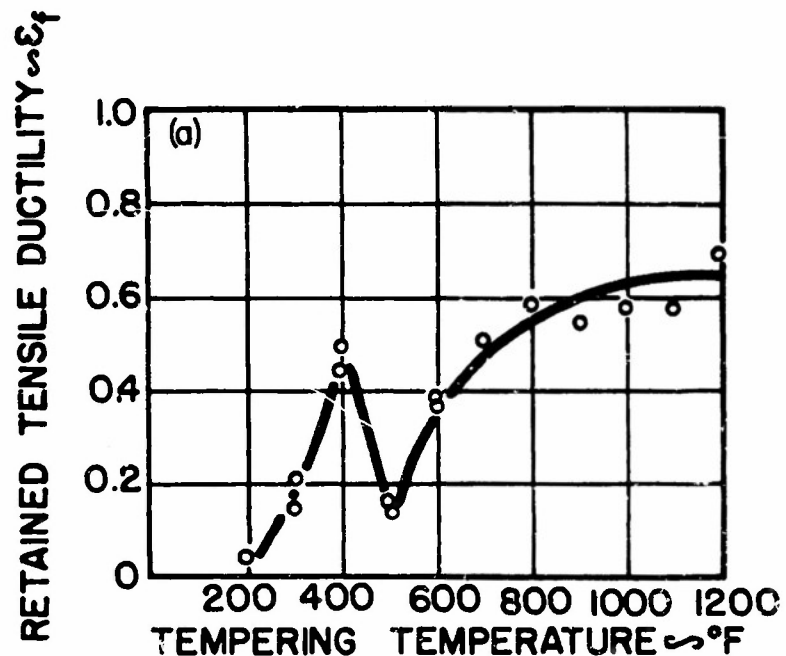
FIG.17: THE EFFECT OF TEMPERING TEMPERATURE UPON
THE TENSILE FRACTURE PROPERTIES OF QUENCHED
AND TEMPERED SAE 1340 STEEL. TEST
TEMPERATURE WAS –321°F.
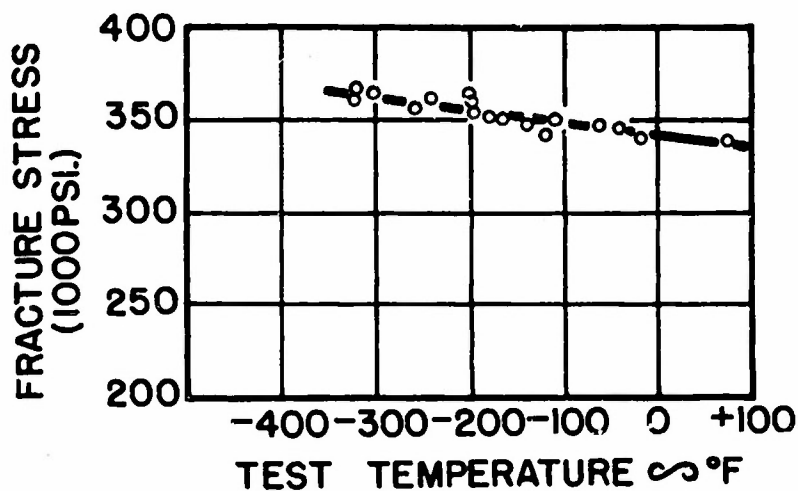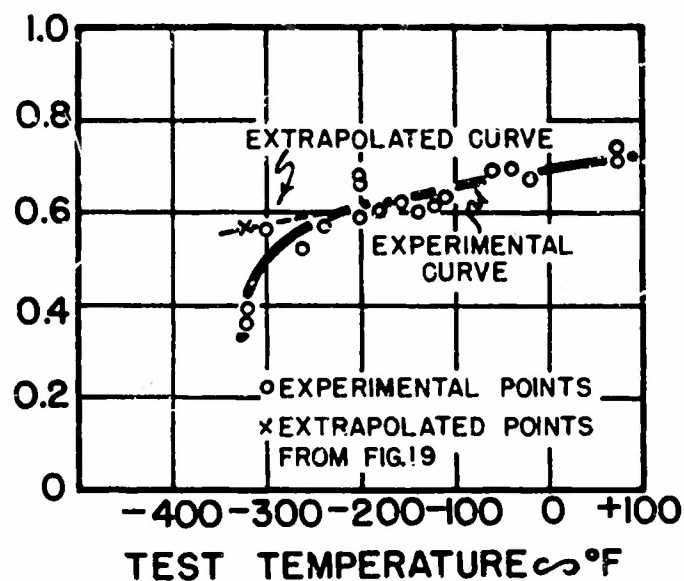
FIG.18 : THE EFFECT OF TEST TEMPERATURE UPON THE
TENSILE FRACTURE PROPERTIES OF SAE 1340
STEEL QUENCHED AND TEMPERED AT 600°F.

FIG. 19: EFFECT OF TEST TEMPERATURE ON THE RETAINED TENSILE DUCTILITY OF QUENCHED AND TEMPERED (600°F) SAE 1340 STEEL SUBSEQUENT TO TENSILE OR TORSIONAL PRESTRAIN (+75°F).

FIG.20: EFFECT OF TORSIONAL PRESTRAIN ON THE
TENSILE FRACTURE PROPERTIES OF ANNEALED
SAE 1340 STEEL.

FIG.21: EFFECT OF TEST TEMPERATURE ON THE RETAINED
TENSILE DUCTILITY OF QUENCHED AND TEMPERED(600°F)
SAE 1340 STEEL SUBSEQUENT TO TENSILE OR
TORSIONAL PRESTRAIN.

FIG.22: EFFECT OF TEST TEMPERATURE UPON THE TENSILE
FRACTURE STRESS OF ANNEALED ELECTROLYTIC
TOUGH PITCH COPPER SUBSEQUENT TO TENSILE
OR TORSIONAL PRESTRAIN(+75°F).

FIG 23: EFFECT OF TEST TEMPERATURE ON THE TENSILE
FRACTURE STRESS OF SPHEROIDIZED SAE 1020 STEEL
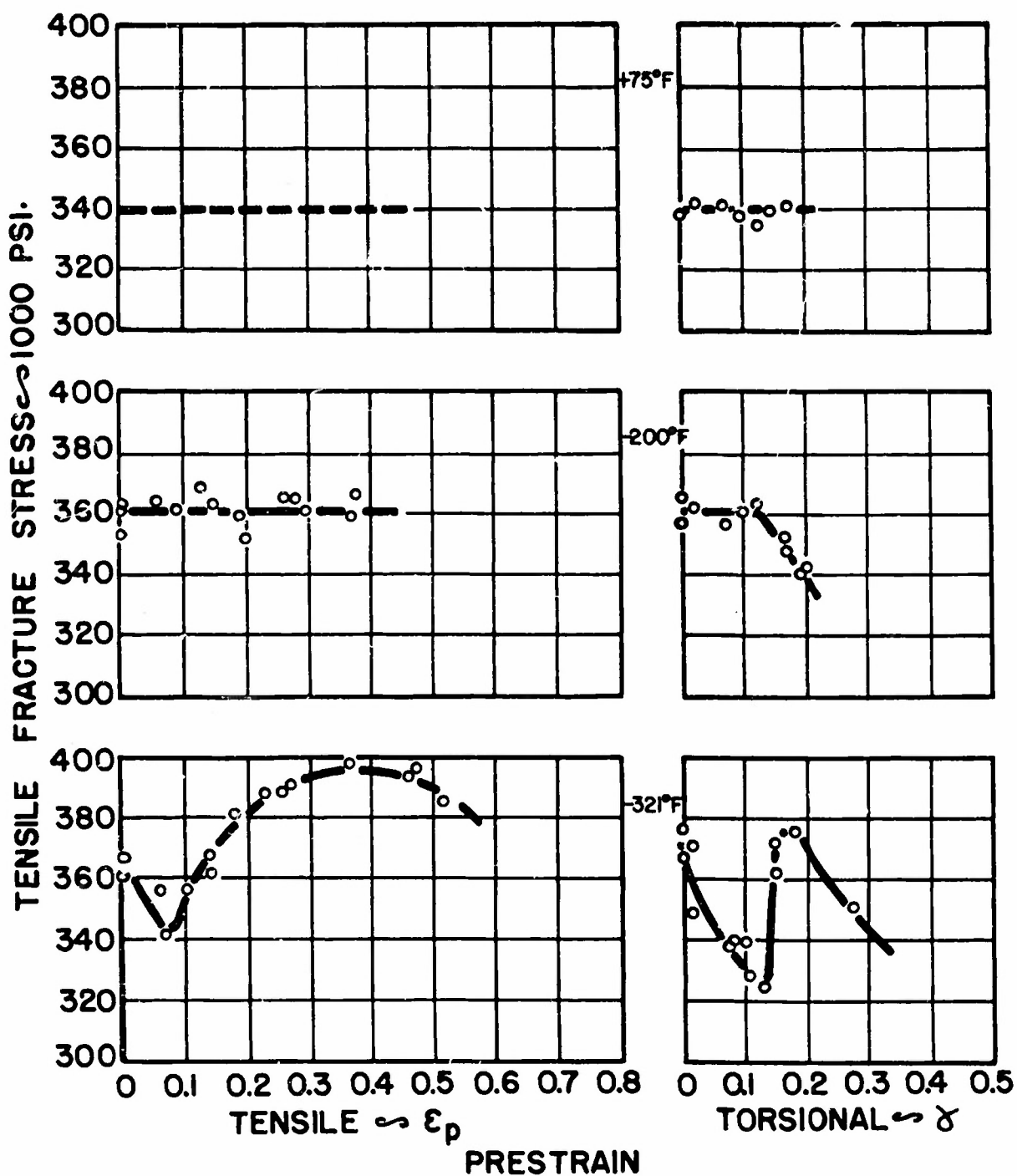SUBSEQUENT TO TENSILE OR TORSIONAL PRESTRAIN.
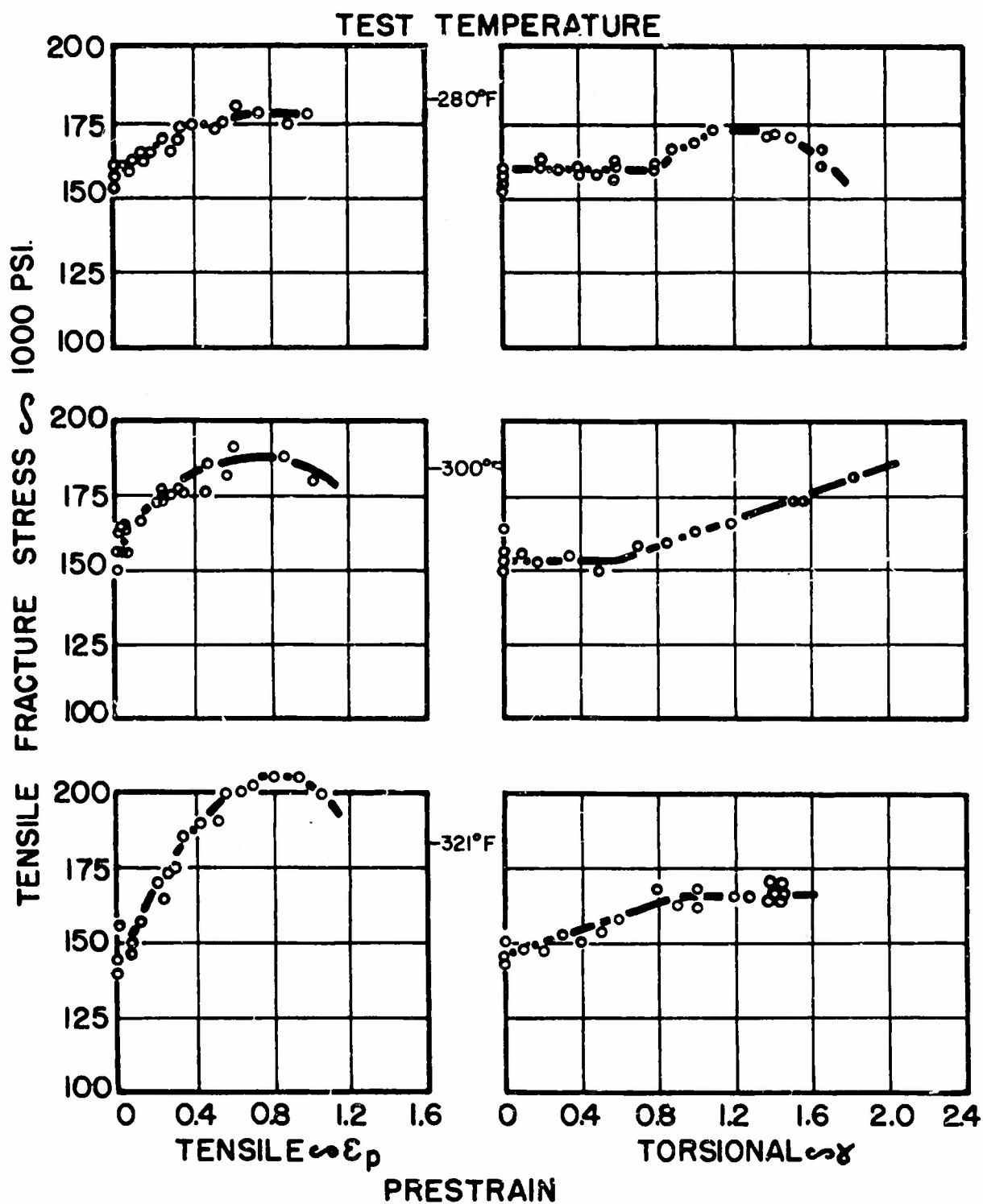
FIG.24: EFFECT OF TEST TEMPERATURE ON THE TENSILE
FRACTURE STRESS OF SPHEROIDIZED SAE 1020 STEEL
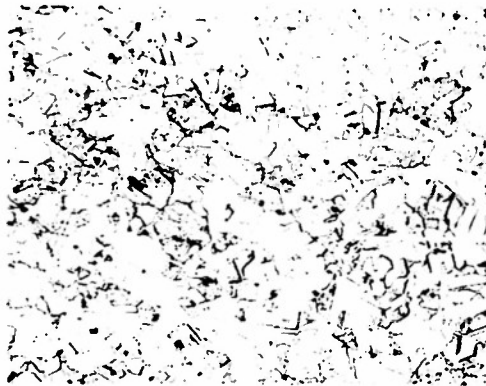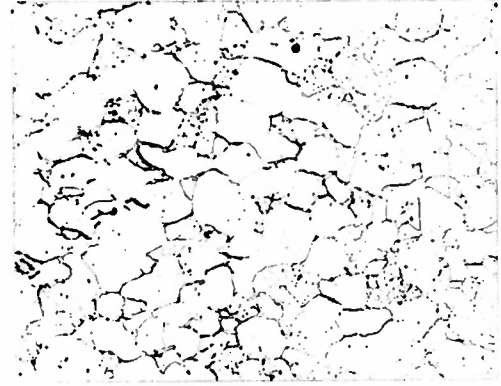SUBSEQUENT TO TENSILE OR TORSIONAL PRESTRAIN.

FIG.25: EFFECT OF TEST TEMPERATURE ON THE TENSILE
FRACTURE STRESS OF QUENCHED AND TEMPERED
(600°F) SAE 1340 STEEL SUBSEQUENT TO TENSILE
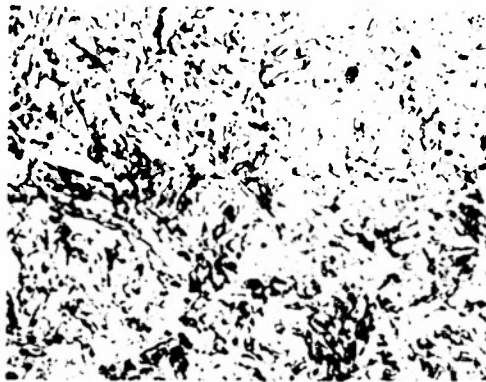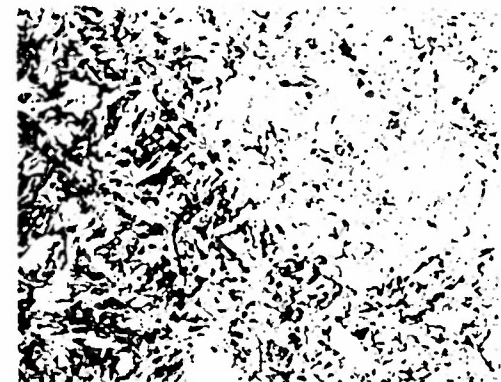OR TORSIONAL PRESTRAIN.

(a) ANNEALED ELECTROLYTIC (b) SPHEROIDIZED SAE 1020
    TOUGH PITCH COPPER   STEEL

         200 X   300 X

(c) TORSION SPECIMEN   (d) TENSILE SPECIMEN

WATER QUENCHED AND TEMPERED (600°F) SAE 1340
STEEL ∿ 1000 X

FIG.26 : MICROSTRUCTURES OF MATERIALS USED IN
         INVESTIGATION.